INSTITUTE FOR DIRECT ENERGY CONVERSION

TOWNE SCHOOL

UNIVERSITY OF PENNSYLVANIA

PHILADELPHIA, PENNSYLVANIA

UNPUBLISHED PRELIMINARY DATA

GPO PRICE $ _____

CSFTI

~~OTS~~ PRICE(S) $ _____

Hard copy (HC) 3.00

Microfiche (MF) .75

STATUS REPORT

INDEC-SR-5

NATIONAL AERONAUTICS AND SPACE ADMINISTRATION

GRANT NSG-316

January 4, 1965

INSTITUTE FOR DIRECT ENERGY CONVERSION

TOWNE SCHOOL

UNIVERSITY OF PENNSYLVANIA

PHILADELPHIA, PENNSYLVANIA

STATUS REPORT

INDEC-SR-5

NATIONAL AERONAUTICS AND SPACE ADMINISTRATION

GRANT NSG - 316

January 4, 1965

ABSTRACT

2. MATERIALS ENGINEERING

2.1 Partial Molar Properties of Magnesium Base Binary Thermal Energy Storage Materials.

This study was undertaken to provide information on TES materials with large heats of fusion where adjustment of melting temperature would be useful. A primary goal was the development of a galvanic cell method to permit rapid and convenient measurement on several alloys in one experiment. Partial molar thermodynamic properties so derived are to be evaluated in a standard computational procedure to yield the heat of fusion as well as a measure of chemical reactivity. The high temperature cell and electrodes have been thoroughly checked and successfully operated with the alloy system Mg-Al, which exhibited negative deviation from ideal behavior, as expected.

2.2 Phase Diagrams of the Systems MgF_2 - MgO, MgF_2 - CaO

Work on determining the temperature-constitution diagrams of mixtures of compounds with high heat of fusion was begun in order to assess the possibility of melting temperature control for TES materials. Sample preparation procedures for the differential thermal analysis equipment were developed and the magnesium fluoride rich regions of the MgF_2--MgO and MgF_2-CaO systems were studied as well as a start made on the MgF_2-Al_2O_3 system. Simple eutectics were formed in all cases: 0.085 mol fraction MgO, 1220 $\pm$ 2°C; 0.075 mol fraction CaO, 1208$\pm$2°C; approximately 4.5 weight percent Al_2O_3, 1250°C.

2.3 Transient Measurement of Thermal Diffusivity of Refractory Materials at High Temperature

The pressing need for systems design engineering data on thermal transport properties of TES materials at high temperature prompted this work. A precise measurement technique which yields apparent thermal diffusivity of solid phase TES materials has been designed for operation at temperatures greater than 2000°C. This technique can be adopted to separate

the photon and phonon contribution to thermal transport, provided the material to be tested can be controlled in terms of its purity, grain size, crystal structure and porosity. The chief problem with existing methods lies in the difficulty of matching actual temperatures with mathematical boundary value requirements. The present method employs a feedback system to control surface temperature according to a predetermined time sequence. Fundamentally, the time lag between the temperatures at the surface and center will be monitored for a constant rate of surface temperature rise. The mathematical treatment has been fully developed and successfully tested experimentally, and the vacuum high-temperature furnace and control system are in final stages of building.

3. PLASMA ENGINEERING

3.1 Emitter Surface Physics of Plasma Diodes

The principal objective of this work is the calculation of the surface charge distribution at a metal-vapor interface. This surface charge distribution will be predicted as a function of the crystallographic structure of the substrate, the number of adsorbed particles, and the fraction of charge associated with the ionic and covalent bonding between the adsorbed particles and the substrate. The solution of this problem is proceeding by using of the statistical methods commonly employed in many body problems.

Several problems of considerable importance to plasma thermionics were investigated in the course of formulation of the above problem with the following findings:

1. Clarification of the concept of a work function. Thermionic researchers have introduced a number of different types of work functions. The significances and interrelationships between these various "work functions" have been studied and clarified. This study has lead to a new definition of the classical concept of a Richardson plot for thermionic emission in a gaseous environment.

2. Development of a new macroscopic model of electron emission from a metal in a gaseous environment has been developed. This theory, which requires no adjustable constant, includes the concepts of the state of maximum activity and its relationship to the Richardson work function. Electron emission S curves have been calculated on the basis of this model for a cesium-tungsten system. These results show excellent agreement (over more than seven orders of magnitude of the cesium arrival rate) with the experiments of Houston and Langmuir and Kingdon.

Preliminary parts of these results are presented in the Institute publication INDEC-12. Details will be published in a forthcoming paper.

3.2 Emitter Sheath Polarity in Plasma Diodes

The purpose of this research was to develop criteria for specification of the polarity (sign) of the emitter sheath in a broad-spaced plasma diode. General criteria that are applicable for all plasma diode spacings have been developed. It has been shown that these general criteria reduce to those criteria presently in common use only for a collisionless plasma diode (electron current/ion current $\lesssim 491$ implies $\pm$ emitter sheath). For a broad-spaced collision-dominated plasma diode, a phenomenological macroscopic model has been used to show that the ratio of the electron emission current to the ion emission current does not uniquely determine the polarity of the emitter sheath. The ned volume ionization and/or recombination and the electron plasma temperature have also been shown to be important. No specific mechanism for volume ionization was assumed; both the net volume ionization and the electron temperature were treated as unknown parameters.

This research is important to an understanding of the operational characteristics of a plasma thermionic converter. It is of particular importance in understanding the characteristics of the passive mode - ignited mode transition. Complete results and details of this research are presented in Institute publications INDEC-11 and INDEC-13.

3.3 Investigation of Na-K Seeded Argon Plasma

The objective of this research is to measure non-equilibrium ionization and its effects in an alkali-metal (Na-K) seeded argon plasma (1 atm. pressure, .04-.36 wt. per cent K). The non-equilibrium ionization is generated by an externally produced electric field. Spectrophotometric measurements are being employed to determine local electron and atom-ion spatial temperature distributions. These spectrophotometric measurements, electrical measurements, and separate measurements of the pressure and chemical composition of the plasma will be used to calculate the local values of electrical and thermal conductivities.

Checkout of the experimental system is near completion. Improvements in the design of the system have been made as a result of problems encountered during checkout.

4. ELECTROCHEMICAL ENGINEERING

4.1 Transient Concentration Variation in Natural Convection Electrolysis

Previous efforts have been directed towards biological fuel cells. Studies on dehydrogenase enzyme systems such as the formic hydrogenlyase reaction of *E. coli* and the lactic dehydrogenase enzyme oxidation of lactic acid have indicated that the direct type of cell reaction involving electron transfer at an electrode may be the exception rather than the rule.

This work, in its overall aspect has pointed to other important problems which exist in the fuel cell area. Chief among these are improvement of the oxygen (air) electrode and development of a rational basis of porous electrode design, based on model studies. To develope the experimental capability for probing local electrolytic mass transport behavior in small model pores, an analysis of the concentration transient (to be related to overpotential) at a planar electrode, following a step in current, has been performed. A means for evaluating the local mass transport boundary layer thickness will follow from the combined analysis. It has been shown that the concentration (and thus the overpotential) transient will be independent

of ultimately induced natural convection modes up to a dimensionless time, τ, of at least 0.125 and possibly up to $\tau = 0.333$, where D = diffusion coefficient, t = time, δ = ultimately established boundary layer thickness.

TABLE OF CONTENTS

LIST OF ILLUSTRATIONS

1. INTRODUCTION

Dr. Manfred Altman, Director

Progress to date should be measured against the overall objectives of the Institute which are:

1. To be a "Teaching Institute," where graduate engineers may be attracted to the broad, interdisciplinary area of Direct Energy Conversion.
2. To provide research opportunities for the staff and graduate students in a multi-disciplinary atmosphere.
3. To explore and develop new courses and curricula towards the production of engineers who will possess the broad understanding of the basic scienee underlying Direct Energy Conversion, but who will be engineering motivated.

The main body of this report is directed to a discussion of our research activities. The first section presents a one-page summary of these activities, and the second part contains the details. The remainder of this introduction is devoted to a discussion of the progress which has been made in addition to the performing of research.

At the present time, the Institute supports thirteen graduate students at various stages of development. Of these, eight are M.E.'s, three are Ch.E.'s, and one each from E.E. and Met.E.

The senior staff has organized along the following lines. Three technical working groups have been formed. These are concerned with Plasma Engineering, Electrochemical Engineering, and Materials

Engineering. Each group has staff members from the various engineering schools, post-doctoral appointees, and at least one working member from industry. Each group takes advantage of the fact that several disciplines are available to formulate new research ideas, and to conceive of new and better ways of conducting the research and teaching functions of the Institute.

Each group is headed by an expert in the appropriate area of Direct Energy Conversion, who is responsible for keeping up with latest developments in the areas of interest to a particular group. This makes it possible to utilize specialists who are not necessarily conversant with Direct Energy Conversion but who, nonetheless, have much to contribute. Research students report their progress to these groups periodically, and the availability of such a critical forum has been found to be most helpful.

This is the third year since the Institute was formed. Since that time, roughly fifty graduate students have been exposed to the problems of Space Power and Energy Conversion. Interest among students, continues to grow, and the staff is developing the competency to work as team members, which is essential to such a broad activity. We feel that we are over the initial growing pains, and that we are now ready to make significant contributions in our chosen field of endeavor.

The Institute, as such, is an attempt to pioneer new and better ways of performing the teaching and research functions of a great university in a specific interdisciplinary area. Every effort is being made to use the Institute as an "overlay" on the existing engineering departments rather than having it become another isolated entity, without real justification to be at a university. An additional aim is to serve the local industrial community in terms of applying space oriented research towards community ends. It was felt that the many problems which are inherent in our efforts to optimize our contribution to the University, to NASA and to industry were such that creative and novel solutions needed to be generated. In order to accomplish this and particularly to establish a good communications channel among the organizations involved, it was decided to form a board of advisors to the Institute. As presently constituted, the board consists of three "industrial" and three "government agency" personnel. This board reports to Dr. Carl C. Chambers, Vice President for Engineering Affairs, University of Pennsylvania.

Representative questions to which this board has addressed itself are:

1. Ways by which the Institute may achieve diversification of funding and support.

2. How to communicate with industry.

3. How to assess the research function of the Institute with education as its primary object.

4. How to provide for administrative and laboratory space.

5. How to integrate Institute personnel within the existing Engineering School structure.

6. How to obtain student fellowships from industrial organizations.

It is planned to publish the results of these activities because the problems and the considerations are general ones and their solution at the University of Pennsylvania may well point the way to similar solutions elsewhere.

2. MATERIALS ENGINEERING

Acting Branch Chief: Dr. Leonard Nanis

Senior Members: Dr. Geoffrey Belton, Dr. Ram A. Sharma

N65 19777

2.1 Partial Molar Properties of Magnesium Base Binary Thermal Energy Storage Systems

Dr. Geoffrey Belton; Y. Rao

Introduction

Magnesium-silicon alloys have been suggested as Thermal Energy Storage materials.[1] The compound Mg_2Si, with a melting point[2] of 1102°C and heat of fusion[2] 270 ± 30 cal/gm seems particularly attractive. Recent measurements[3] of the thermal conductivity of Mg_2Si, although valid only up to 277°C, indicate further suitability for TES applications. In units of cal cm^{-2} $(°C)^{-1}$ sec^{-1} cm^{-1}, the thermal conductivity of Mg_2Si was found to be 0.0186 at 27°C and 0.01 at 277°C. The value for MgO[4a] is 0.006 at 1000°C, while purely for the sake of comparison, the value for Type 304 stainless steel[4b] near room temperature is 0.029. The favorable thermal conduction properties of Mg_2Si suggest that increased attention be given to similar intermetallic compounds.

It is clearly desirable to accelerate the acquisition of heat of fusion data for binary metal systems such as Mg-Si. The thermodynamic relations between heat of fusion and partial molar mixing quantities, pointed out by Rao and Belton[5] afford the possibility of such a rapid method, based on a galvanic cell technique. The measurement of the partial molar free energy and entropy from the

potential and its temperature variation for a virtual concentration cell involving a pure metal and an alloy as electrodes is well known. The additional information concerning thermodynamic activity of the components of the alloy system is of further advantage in evaluating chemical stability of TES container materials. Further virtues of the galvanic cell method are essentially experimental but are non-trivial. In particular, a large number of alloys may be measured at one time in apparatus which is of convenient size. The inherent precision of electrical measurements as contrasted with e.g. calorimetric methods is an additional advantage.

In preparation for galvanic cell measurements on the Mg-Si system, the electrolyte chosen ($MgCl_2$-$CaCl_2$) and overall system were checked by a study of the Mg-Al system in the range 700-900°C. A unique feature of the cell is the inclusion of a reversible chlorine electrode for continual checking of the condition of the pure magnesium electrode by means of the expected constant potential difference between the pure magnesium and chlorine electrodes.

EXPERIMENTAL

Equipment:

The resistance furnace was made by winding 0.020" diameter Pt - 10% Rh wire on a 30" x 2" diameter alumina tube and enclosing it in a

transite casing filled with insulating alumina powder. This furnace can be heated up to 1500°C. A Wheelco model 407 temperature controller in conjunction with a silicon controlled rectifier is used to regulate the power input to the furnace to obtain constant temperature. A Leeds & Northrup K-3 potentiometer and Keithely 610A electrometer were used for potential measurement. A constant current source is used to perturb the cell to check the attainment of true equilibrium.

A description of the electrolytic cell was given in the previous report.(6) The electrode assembly consists of:

1. Pure magnesium electrode
2. Magnesium - Aluminum alloy electrode
3. Chlorine electrode

These electrodes and a thermocouple were fixed in a No. 9 1/2 rubber stopper that fits into the cell.

Materials:

Available solid magnesium chloride contains six waters of hydration. Various methods have been tried to produce the anhydrous salt. Attempts to dry the salt under vacuum while raising the temperature slowly to about 450°C were unsatisfactory because of the hydrolysis reaction ($MgCl_2 + 2H_2O = Mg(OH)_2 + 2\ HCl$). Therefore, a method of heating the hydrated salt with gross amounts of NH_4Cl

in a pot furnace was tried. Ammonium chloride dissociates at about 340°C according to ($2\ NH_4Cl \longrightarrow 2\ NH_3 + 2\ HCl$). This excess hydrogen chloride reverses the hydrolysis reaction.

Pure anhydrous $MgCl_2$ was obtained. This pure salt was stored in a dry box. The same procedure was used to procure dry calcium chloride.

Pure reagent grade magnesium was obtained in the form of rods from Fisher Scientific Co. Pure Al wire was also obtained from the same source. Magnesium - Aluminum alloys were prepared in an induction furnace using graphite crucibles under an argon atmosphere. Spectroscopic quality graphite rods 1/8" x 12" long were obtained from the Ultra Pure Carbon Co., Michigan.

Experiment:

Anhydrous magnesium chloride was transferred from the dry box to the cell. The cell was placed in the resistance furnace and was slowly heated under a dry argon atmosphere. When the salt was molten, the electrode assembly was carefully lowered into the cell. Pure magnesium and magnesium-aluminum alloy were added to the respective electrode compartments. Chlorine gas, dried over anhydrous magnesium perchlorate was passed through the chlorine electrode at the rate of 8 ml/min. Measurements of galvanic potential between pure magnesium-chlorine electrodes and that between Mg-Al

alloy-chlorine electrode were taken over a range of temperatures. About 10 hours were allowed for the initial attainment of equilibrium for the chlorine electrode. After each temperature change, about 1.5 - 2 hours were allowed for the attainment of a new steady potential. The criterion of stability was a variation of less than 0.8 mV per hour.

Electrolyte components, $MgCl_2$ and $CaCl_2$, were carefully weighed in a dry box, mixed and transferred to the cell and a procedure similar to that for pure salt was followed.

Results and Discussion:

Measurements of the electromotive force at various temperatures of the cells of the type

$$Mg(l) \mid MgCl_2(l) \mid Cl_2(g)$$

$$Mg\text{-}Al(l) \mid MgCl_2(l) \mid Cl_2(g)$$

permit the calculation of the thermodynamic properties of the reactions.

$$Mg(l) = Mg^{++} + 2e^-$$

$$Cl_2(g) + 2e = 2Cl^-$$

$$Mg(l) + Cl_2(g) = Mg^{++} + 2Cl^- = MgCl_2 \qquad \text{I}$$

$$Mg \text{ (in alloy) } (l) + Cl_2(l) = MgCl_2 \qquad \text{II}$$

Reaction I is known as the formation cell reaction and since all the substances are in standard state and the e.m.f. is written as E° in Eqn. 2.1-1

$$\Delta F^{\circ} = -NFE^{\circ} \qquad (2.1\text{-}1)$$

where ΔF° = Standard free energy of formation of pure $MgCl_2(l)$, cal mol^{-1}

N = Number of electrons transferred = 2

F = Faraday's constant

= 23066 cal/volt-equiv.

E° = Standard potential in volts.

For reaction II

$$\Delta F = -NFE \qquad (2.1\text{-}2)$$

where ΔF = Free energy of reaction cal/mol

E = Potential between the alloy-electrode and chlorine electrode, volts.

The free energy of Reaction II may also be expressed as

$$\Delta F = \Delta F^{\circ} + RT \ln K \qquad (2.1\text{-}3)$$

where

$$k = \frac{a_{MgCl_2}}{a_{Mg(alloy)} P_{Cl_2}} \qquad (2.1\text{-}4)$$

The equilibrium constant (Eq 2.1-4) for Reaction II where chlorine

and pure magnesium chloride are in standard states becomes simply

$$K = \frac{1}{a_{Mg\,(alloy)}} \qquad (2.1\text{-}4a)$$

Combination of Eqns 2.1-1, 2.1-2, 2.1-3 and 2.1-4a yields

$$\log a_{Mg\,(alloy)} = \frac{-NF(E^\circ - E)}{2.3RT} \qquad (2.1\text{-}5)$$

Table 2.1-1 shows typical data obtained for an alloy with Mg mol fraction equal to 0.6864 at various temperatures. It may be seen that sufficient precision is available so that the potential difference clearly resolves the usually difficult-to-obtain temperature variation from which the entropy of mixing is calculated.

TABLE 2.1-1

Potential Data, Mol Fraction Mg = 0.6864

Temp, °C	E°, volt	E, volt	$(E^\circ - E)$, mV
709	2.4842	2.4585	25.70
736	2.4554	2.4309	24.50
800	2.4122	2.3898	22.38
810	2.4052	2.3832	22.00
862	2.3760	2.3557	20.31

A plot of activity vs. mol fraction for magnesium at 800°C is shown in Fig. 2.1-1. The negative deviation from ideal behavior

is expected for the Mg-Al system because of extensive solid compound formation. Thus the overall method for obtaining thermodynamic data leading to an evaluation of heat of fusion in metal alloy systems is considered to be thoroughly checked and ready for investigation of the Mg-Si and other systems.

Work still needed on the Mg-Al system concerns data for dilute concentrations of Mg in Al followed by Gibbs-Duhem integration of Mg activity in order to obtain the activity of aluminum and finally evaluation of fusion heats. Work is already underway for the construction of a cell made completely of alumina for investigation of the Mg-Si system.

References

1. Status Report, Nov. 15, 1962 Institute for Direct Energy Conversion, Univ. of Penna. NSG 316, p. 10.
2. O. Kubaschewski, E. L. Evans, "Metallurgical Thermochemistry" J. Wiley, N. Y., 1956.
3. R. LaBetz, M. Donald, J. Electrochem. Soc. V. 110, p. 121 (1963).
4. ASM Metals Handbook, 1948, (a) p. 28, (b) p.26.
5. G. R. Belton, Y. K. Rao, The Binary Eutectic as a Thermal Energy Storage System: Equilibrium Properties, presented at 6th National Heat Transfer Conference, Boston, Mass.
6. Status Report, August 10, 1964, Institute for Direct Energy Conversion, Univ. of Penna. NSG 316, p. 22.

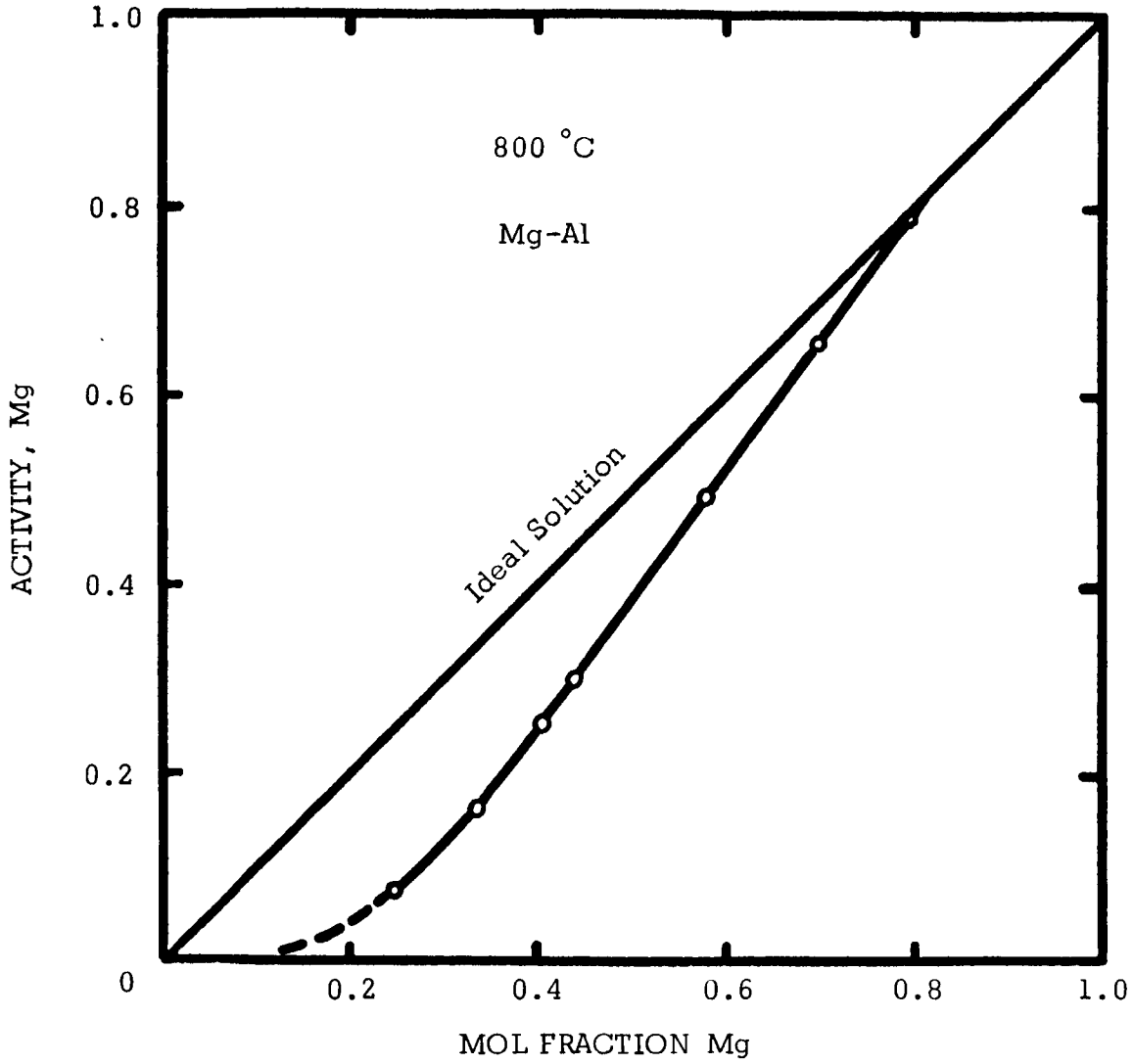
1.0
0.8
0.6
0.4
0.2
0
ACTIVITY, Mg
800 °C
Mg-Al
Ideal Solution
0.2
0.4
0.6
0.8
1.0
MOL FRACTION Mg

Figure 2.1-1.

2.2 Phase Diagrams of the Systems MgF_2-MgO, MgF_2-CaO

Dr. Geoffrey Belton, Dr. Ram A. Sharma

Flexibility in the use of magnesium fluoride as a thermal energy storage material can be obtained through control of the melting temperature by the addition of other components to form binary systems. The acceptably large values of the heat of fusion of calcium oxide and magnesium oxide prompted an investigation of the phase diagrams of the binary systems MgF_2-CaO and MgF_2-MgO by the method of differential thermal analysis.

A description of the apparatus and control circuitry designed for this purpose, together with preliminary calibrating experiments were presented in an earlier report.(1)

High purity magnesium fluoride (Mallinckrodt Co. electronic grade) was dried by heating slowly to approximately 400°C under a vacuum of 10^{-3} mm Hg and held at that temperature until gas evolution ceased. After cooling, about 25% by weight of ammonium fluoride was mixed with the salt and the mixture, contained in a platinum crucible, was heated slowly to 200°C under an inert atmosphere and held for about 6 hours. The temperature was then raised to 700°C to allow decomposition and volatilization of the excess ammonium fluoride. The container was then cooled and opened under dry argon.

Microscopic examination of a melted and cooled sample of the fluoride prepared in this way showed it to be a single-phase material with no evidence of a magnesium oxide phase. Samples prepared from material not subjected to the ammonium fluoride treatment showed evidence of fine MgO needles in the MgF_2 matrix of the type shown in Fig. 2.2-2.

Magnesium oxide, for the preparation of MgF_2-MgO mixtures, was prepared by igniting Analar grade magnesium carbonate at 1200°C for three hours.

Samples for differential thermal analysis were prepared by mixing together the finely ground materials in the desired proportions, and melting together at about 1280°C. Thermal arrests on cooling and heating were determined at a variety of rates between 1/4° and 2° per minute. The results are presented in Fig. 2.2-1, where the error limits shown represent maximum deviation in the experimental results. When no error limit is shown, successive experiments yielded data within $\pm$ 1°C. The phase diagram is the simple eutectic, with the eutectic composition at 0.085 mol-fraction of MgO and a eutectic temperature of 1229 $\pm$ 2°C.

Micrographic examination of the samples taken from the MgF_2-rich components showed needles of MgO in a matrix of MgF_2 (eutectic composition) with no sign of irregular grains of MgO which could

be an indication of undissolved MgO.

Samples taken from the MgO-rich side of the system showed grains of MgO as well as needles. The possibility exists that the grains represent some undissolved MgO as well as the formation of crystals of MgO. Because of this, the liquidus curve for the MgO-liquid reaction is only tentatively drawn (Fig. 2.2-2), based on an estimate of the enthalpy.(2)

Similar experiments were carried out on the binary system MgF_2-CaO, the CaO being prepared by ignition of reagent grade calcium carbonate at 1200°C. for four hours. A simple eutectic system was again found. The experimental results and derived phase boundaries are shown in Fig. 2.2-3. The eutectic composition and temperature are respectively 0.075 mol-fraction CaO at 1208 $\pm$ 2°C. A photomicrograph of the eutectic composition is shown in Fig. 2.2-4 where needles of the oxide may be seen in the fluoride matrix.

X-ray diffraction studies will be carried out on the cooled samples to see if there is any separation of CaO and alteration of the lattice parameters of MgF_2, which would be indicative of the importance of the exchange reaction

$$MgF_2 + CaO = MgO + CaF_2$$

The depression of the freezing point shown in Fig. 2.2-3 is almost exactly double that of the MgO system. This indicates that CaO is

completely dissociated as would be expected, and supports the interpretation of the data as a true binary system MgF_2-CaO.

Preliminary measurements for the system MgF_2-Al_2O_3 are presented in Fig. 2.2-5 and a photomicrograph of the eutectic structure is shown in Fig. 2.2-6. The structure is one of Al_2O_3 grains in a matrix of MgF_2. Studies of this system were undertaken to assist in the interpretation of the MgF_2 based systems. The system is not thermodynamically stable and over periods of about 20 hours, AlF_3 is evolved and the system reverts back to the MgO-MgF_2 system. The data shown were obtained in short-time experiments and probably represent the real quasi-stable MgF_2-Al_2O_3 system. The depression of the freezing point indicates non-dissociation of Al_2O_3.

References

1. Status Report, Institute for Direct Energy Conversion, Univ. of Penna. NSG 316, Feb. 28, 1964, p. 61.
2. JANAF Tables

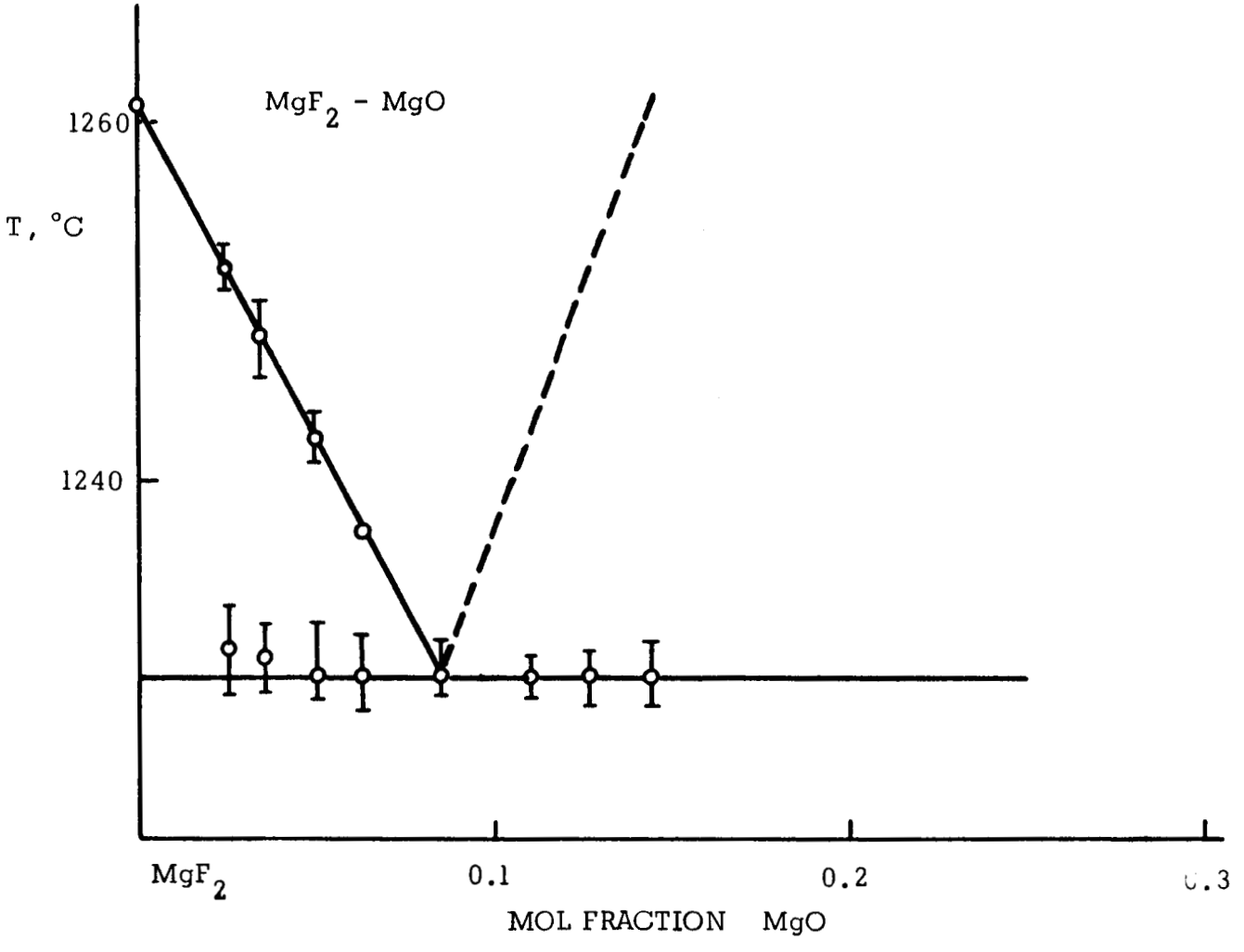

Figure 2.2-1.

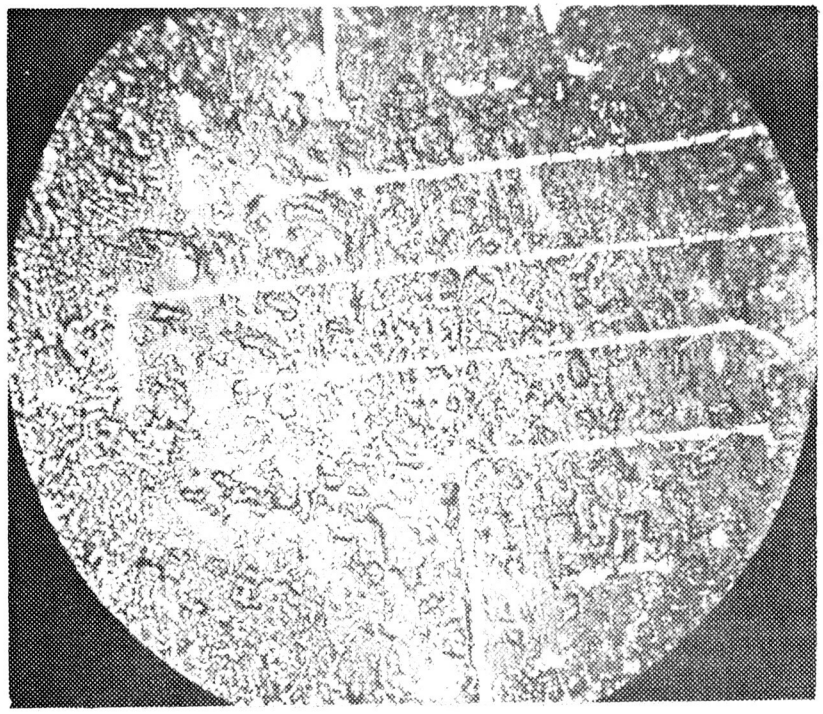

Figure 2.2-2 MgF_2 - MgO eutectic composition 500X

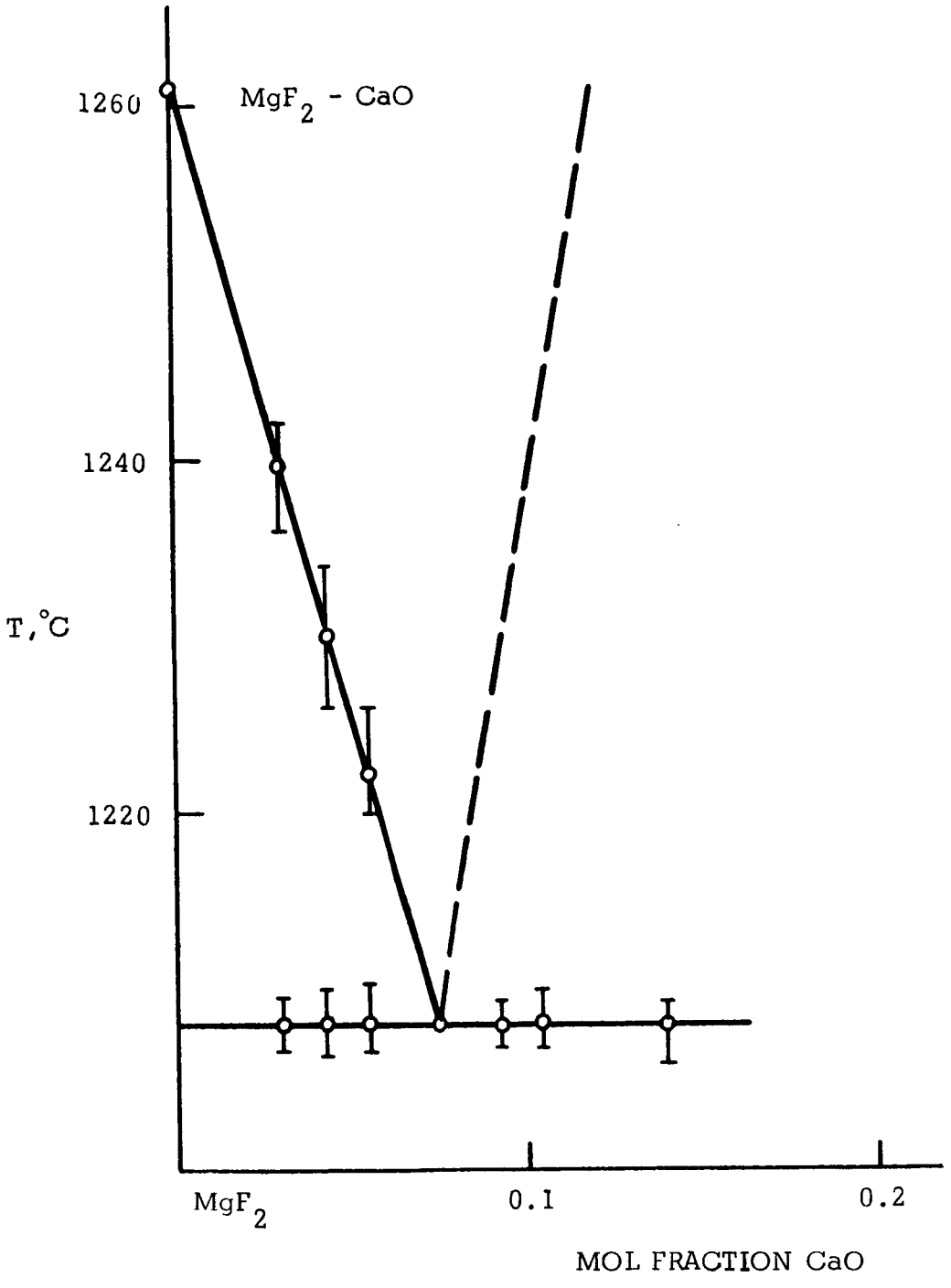

Figure 2.2-3.

Figure 2.2-4 MgF_2-CaO eutectic composition 500X

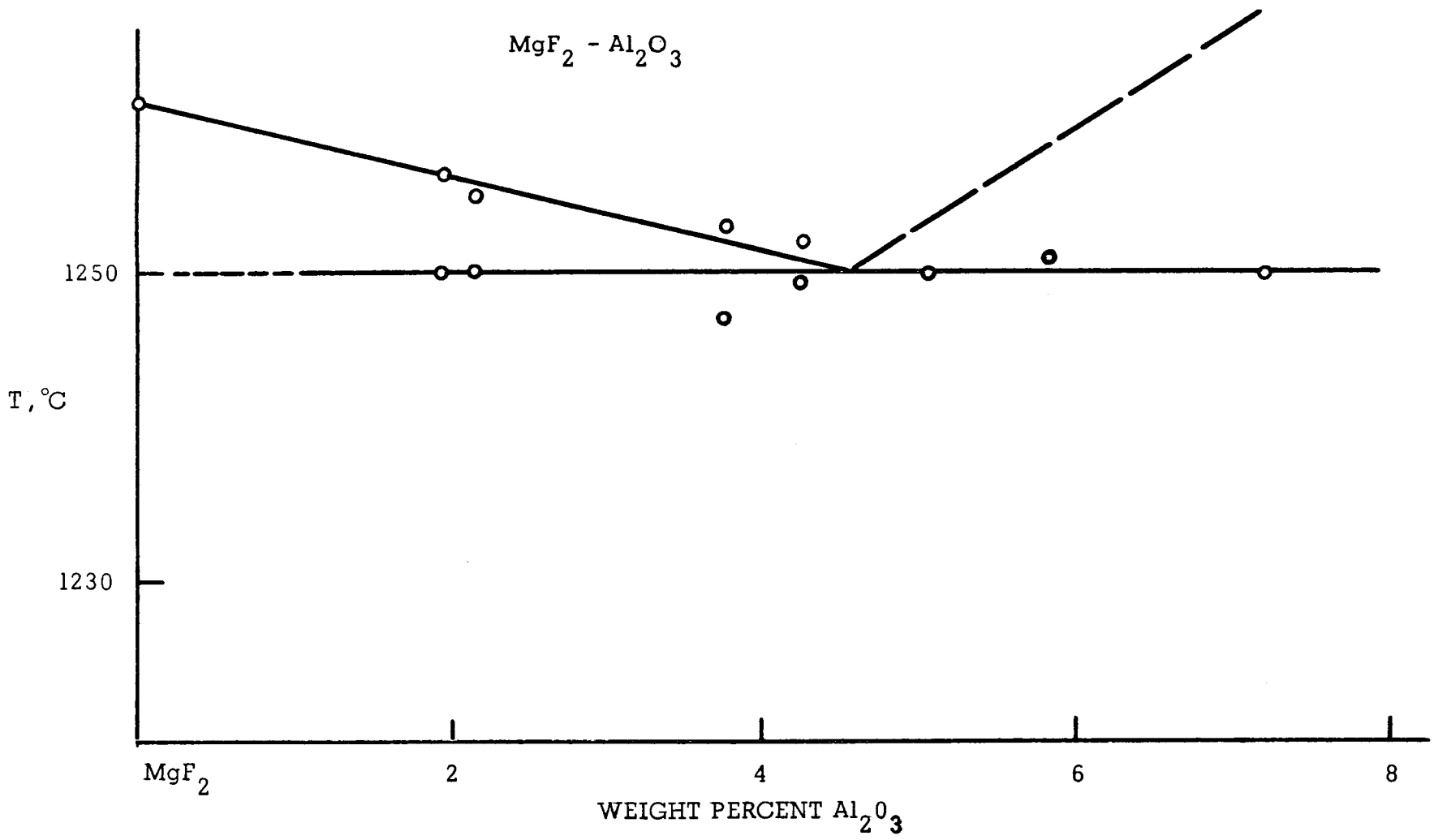

Figure 2.2-5.

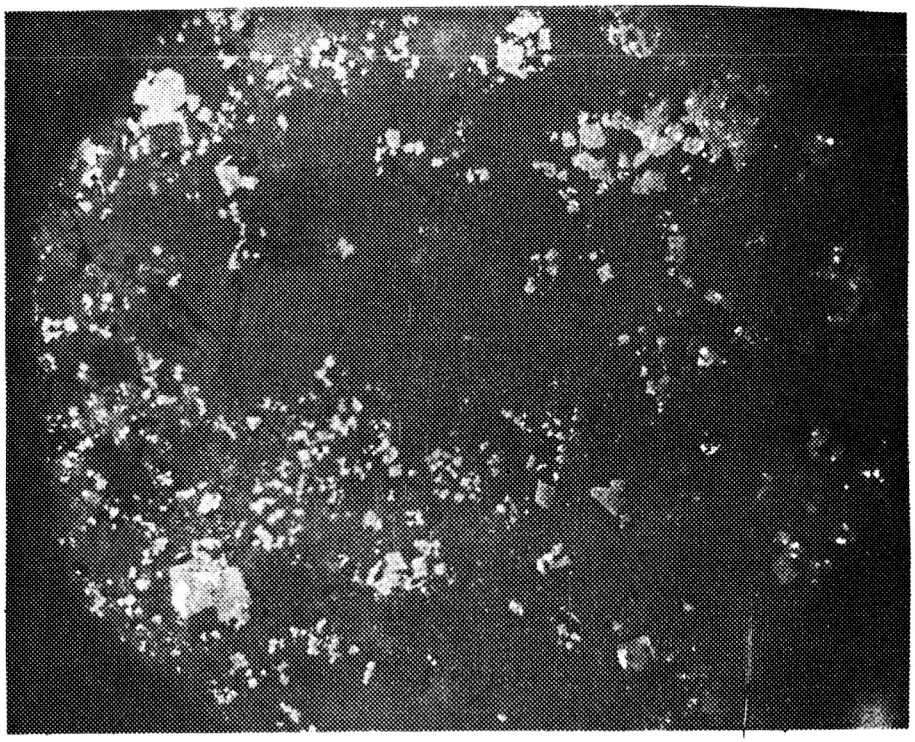

Figure 2.2-6 MgF_2-Al_2O_3 eutectic composition 250X

2.3 Transient Measurement of Thermal Diffusivity of Refractory Materials at High Temperature

Dr. Manfred Altman; H. Chang

A transient technique for the measurement of the apparent thermal diffusivity of refractory materials at high temperature has been developed.(1) The transient method employed requires no measurement of heat flux and no steady-state conditions, both of which are difficult to obtain accurately, especially for poor conductors. An additional advantage of the present transient method is that results may be obtained rapidly and refractory oxides may be measured without containers where thermal error would be introduced. The literature abounds with transient techniques for the measurement of thermal diffusivities of refractory materials at high temperature.(2) The accuracy of the results obtained by these methods depends on how closely the actual test conditions approach the assumed theoretical conditions and on the magnitude of the errors involved in the various experimental measuring devices. Difficulty in matching the mathematically specified boundary conditions exactly has been the major source of error with previous methods. The present method imposes a boundary condition which can be experimentally realized and precisely monitored through the use of an electrical feed-back system.

The method consists of heating the outer surface of a long

cylindrical sample from an initial temperature T_i to a final temperature T_f in a given time interval, Δt, at a constant rate of temperature increase. The transient temperature rise along the axis of the cylindrical sample from the same initial temperature T_i is fixed by its geometry and its diffusivity. The difference in temperature rise between the surface and the axis of the sample as a function of time is utilized for the measurement of diffusivity.

The diffusion equation[3] governing the radial heat conduction in an infinite solid cylinder having radius a, and constant thermal diffusivity α is

$$\frac{\partial \theta}{\partial t} = \alpha\left(\frac{\partial^2 \theta}{\partial r^2} + \frac{1}{r}\frac{\partial \theta}{\partial r}\right); \quad 0 < r < a \qquad (2.3\text{-}1)$$

where θ = Temperature rise from initial temperature (°C) = $T - T_i$

T = Temperature (°C)

T_i = Initial temperature at $t = 0$

r = Radius (cm)

a = Maximum radius (cm)

α = Diffusivity (cm^2/sec)

The solution to equation 2.3-1 is

$$\frac{\theta}{c} = \left(t - \frac{a^2 - r^2}{4\alpha}\right) + \frac{2}{a\alpha}\sum_{n=1}^{\infty} e^{-\alpha Z_n^2 t}\,\frac{J_0(rZ_n)}{Z_n^3 J_1(aZ_n)} \qquad (2.3\text{-}2)$$

where c = the constant rate of temperature increase ($^{o}C/sec$)

J_o = Bessel function of order zero of the first kind

J_1 = Bessel function of order one of the first kind

for the applied boundary and initial conditions

$$\theta = ct;\ r = a,\ t = t$$
$$\theta < \infty;\ r = 0,\ t = t$$
$$\theta = 0;\ 0 \leq r \leq a,\ t = 0 \qquad (2.3\text{-}3)$$

Newman[4] has shown that conditions of heat transfer at the center section half-way from the ends do not differ substantially from that of an infinite cylinder if the length to diameter ratio of the sample is greater than four. In testing homogeneous and isotropic materials, the assumption that diffusivity is a function of temperature only is valid. For mathematical convenience, the assumption that diffusivity is independent of temperature is approximated by measuring small differences in temperature rise between the axis and the outer surface of the specimen. This imposes an upper limit for the value of the temperature differential.

Due to the inaccuracies of the temperature measuring device (i.e. pyrometers are accurate within 1/2% at 2000^{o}C) there also exists a lower limit for the difference in the temperature rise. A balance is therefore necessary.

It is possible, however, after the measurements on diffusivities are made, to obtain a first approximation of α as a function of the temperature and to substitute this into the diffusion equation with $\alpha = f(T)$. An analog computer may then be employed to yield a more accurate value for the diffusivity. The number of iterations required for improvement of α depends on the accuracy desired.

A sample calculation at the end of this section indicates that for an infinitely long MgO specimen, having 2" diameter, 3.40 gm/cc bulk density, 0.25 Cal/gm C° specific heat,[5] 0.02 Cal cm/sec. cm^2 C° thermal conductivity at 800 C° and therefore 2.3×10^{-2} cm^2/sec diffusivity at 800 C°,[6] the solution to equation 2.3-1 with the conditions specified by equation 2.3-3, can be accurately approximated by the first term of equation 2.3-2 after 150 sec. from t = 0. The second term in equation 2.3-2 contributes only 4.23% of the entire solution at t = 150 secs. Equation 2.3-2 with the second term deleted, for the MgO characteristics listed above, or for any material with a thermal diffusivity which is greater than 2.3×10^{-2} cm^2 sec^{-1} for a sample of similar size, is

$$\frac{\theta}{c} = t - \left(\frac{a^2 - r^2}{4\alpha}\right) \text{ for any } t \geq 150 \text{ secs.} \qquad (2.3\text{-}4)$$

Equation 2.3-4 provides two methods for calculating the diffusivity once the temperature rise from T_i for both the surface and the axis

is measured as a function of time (see Fig. 2.3-1).

Method 1. The thermal diffusivity α is inversely proportional to the difference in the temperature rise between the surface and the axis of the sample at any given time t > 150 secs. Equation 2.3-4 may be used to calculate $(\theta_a - \theta_o)$ for an arbitrary $t_1 >$ 150 secs. This yields

$$\frac{(\theta_a - \theta_o)_{t_1}}{c} = t_1 - \left(t_1 - \frac{a^2}{4\alpha}\right) = \frac{a^2}{4\alpha}$$

$$\alpha = \frac{a^2 c}{4} \frac{1}{(\theta_a - \theta_o)_{t_1}} \qquad (2.3\text{-}5)$$

where $\theta_a = T - T_i$ at r=a; the surface of the specimen.

$\theta_o = T - T_i$ at r=o; the axis of the specimen.

Method 2. The thermal diffusivity, α, is inversely proportional to the time increment $(t_1 - t_2)$, where t_1 = 150 seconds (note t_1 is arbitrarily chosen provided it is greater than or equal to 150 seconds) and t_2 is the time elapsed for θ_a to reach the value of θ_o at time t_1. Equation 2.3-4 yields the time increment $(t_1 - t_2)$ when $(\theta_a)_{t_2} = (\theta_o)_{t_1}$.

$$(\theta_a)_{t_2} = (\theta_o)_{t_1} = c t_2 = c\left(t_1 - \frac{a^2}{4\alpha}\right); \quad (t_1 - t_2) = \frac{a^2}{4\alpha}$$

$$\alpha = \frac{a^2}{4} \frac{1}{(t_1 - t_2)} \qquad (2.3\text{-}6)$$

The apparatus consists basically of a high-temperature heating

element, a vacuum chamber to house the heating element, the power supply to the heating element, an electrical feed-back system to regulate the input power to the heating element, and temperature measuring and recording devices to monitor the temperature of the test sample.

The heating element is a 4" diam., 20" long tungsten-mesh cylinder made by Sylvania. The heating element can be operated at a temperature up to 2300°C on a 3 phase A.C. 440 volt, 40 KVA power source. The tungsten-mesh element by-passes the difficulty of tungsten sheet embrittlement. The heating element is enclosed by 10 side, top and bottom radiation shields. The five inner shields are made out of 0.005" tungsten and the five outer shields are made out of 0.002" tantalum.

The heating element is hung by the three tantalum current-carrying leads (see Fig. 2.3-2) which are rigidly attached to the top of the heating element. The three current-carrying leads extend radially outward from the top of the cylindrical element and are set 120° apart from each other. These leads are then supported by three copper water cooled electrodes. The heating element and its radiation shields are placed in a water-cooled copper shell, while the current-carrying leads protrude through the shell. Their ends are clamped to the water-cooled electrodes. The entire assembly is placed in an electro-polished double-wall stainless

steel vacuum tank. The water-cooled copper electrodes are connected to three feed-throughs on the ports of the vacuum tank which connect directly to the leads for in-coming power. Four sight ports fitted with optical quartz are located on the vacuum tank; their locations are shown in Fig. 2.3-2. Other ports placed on the vacuum tank lead to the pumping system and provide for thermocouple feed-throughs.

A steady vacuum of 1×10^{-5} torr is maintained by a pumping system through the pumping port while the heater is in operation at 2300°C. This is accomplished by a Welch 1397 mechanical pump and an NRC-1500 diffusion pump. A liquid nitrogen cold trap, NRC type 014-6 and a molecular sieve foreline trap are used to prevent back streaming.

The power supply to the heating element and the electric feed-back system are shown schematically in Fig. 2.3-3. The heating element is designed to operate at approximately 20 volts with a maximum current of 1440 amps in each phase.

The total power required is then:

$$P = \sqrt{3}\, EI \cos\theta = \sqrt{3}(20)(1440)(.08) = 40 \text{ KVA}.$$

where E is the line to line voltage, I is the line to line current, and $\cos\theta$ is the power factor.

Power is supplied from a 4 line, 3 phase Y-connected AC generator at 440 volts to a three-phase Barber-Coleman silicon-controlled rectifier, 621A-27760-173. The power output from the rectifier is

then fed into the primary windings of three Atlantic single phase 20 KVA transformers.

The impedence factor of the transformers is specified at not below 2%. Care must be taken in matching the impedence of the secondary of the step-down transformer to that of the heating element such that maximum power transfer may be effected from the secondary of the transformer to the heating element. The power output of the silicon-controlled rectifier is regulated by an electrical feed-back system, which consists of a Corning precision deviation-controller (series 8810) and a Data-Trak curve-follower programmer.

The rectifier is regulated by a D.C. voltage error function fed in by the Corning deviation-controller. The error function from the controller is the difference between the DC voltages generated by a programmer (the Data-Trak curve-follower) and that produced by an automatic optical-brightness pyrometer (Pyro-Eye-650). The output voltage of the programmer represents the desired temperature rise on the surface of the sample while the output voltage of the optical pyrometer represents the actual measured temperature on the surface of the sample in test. By this arrangement, it is possible to increase the temperature of the heating element at a constant maximum rate of 300°C/min. This is sufficient to raise the temperature of the surface of the cylindrical sample, which is placed in the center of the heating element, at a rate such that

the difference in temperature rise between the surface and the axis of the sample can be precisely measured. The Barber-Coleman rectifier will hold load voltage to within 1.5% for a 10% line voltage variation and has a maximum current limiting feature for short-circuit protection.

Preliminary calculations on vaporization of metallic oxides and reactions of tungsten in vacuum at high temperature indicate that tests may be run up to 1500°C without difficulty; however, until some experimental results are obtained it will not be possible to determine the ultimate temperature under which the tests can be conducted.

Sample Calculation of the temperature of an infinitely long MgO specimen:

The series solution for the temperature $\theta(r,t)$ given by Eqn. 2.3-2 for $\alpha = 2.3 \times 10^{-2}$ cm^2 sec^{-1} for MgO (at 800°C) has been calculated for r = 0 (at the center) and for t = 0, 50, 100, 150, 200, 250 seconds. Substituting the values of a, r, α, in Eqn. 2.3-2 gives

$$\frac{\theta(0,t)}{c} = (t - 70.07) + 560.54 \sum_{n=1}^{\infty} \frac{\exp(-\alpha z_n^2 t)}{z_n^3 J_1(z_n)}$$

The first five terms of the series have been considered in the calculation. The values of (t - 70.07) and $\frac{[560.54 \exp(-\alpha z_n^2 t)]}{z_n^3 J_1(z_n)}$

for various values of t are listed in Table 2.3-1.

TABLE 2.3-1

t	(t-70.07)	$\frac{560.54\exp(-\alpha z_1^2 t)}{z_1^3 J_1(z_1)}$	$\frac{560.54\exp(-\alpha z_2^2 t)}{z_2^3 J_1(z_2)}$	$\frac{560.54\exp(-\alpha z_3^2 t)}{z_3^3 J_1(z_3)}$
0	-70.07	77.635	-9.7926	+ 3.1861
50	-20.07	34.93	-0.04269	$+ 5.1 \times 10^{-6}$
100	29.93	9.875	-0.000186	$< 10^{-7}$
150	79.93	3.532	-7.836×10^{7}	$< 10^{-7}$
200	129.93	1.258	$< 10^{-7}$	$< 10^{-7}$
250	179.93	0.4472	$< 10^{-7}$	$< 10^{-7}$

The remaining two terms for θ (0.0) are - 1.4709 and 0.8156, and for θ (0,150) = 79.93 + 3.532 - 7.838×10^{-7} = 83.462.

It is seen that the first term of the infinite series in Eqn. 2.3-2 contributes 4.23% of total value for θ (0.150).

Furthermore, Equation 2.3-5 yields

$$(\theta_a - \theta_o)_{t_1} = \frac{ca^2}{4\alpha} = \frac{4/3}{4 \times 3.568 \times 10^{-3}} = 93.5^{\circ}C$$

and equation 2.3-6 yields

$$(t_1 - t_2) = \frac{a^2}{4\alpha} = \frac{1}{4 \times 3.568 \times 10^{-3}} = 70 \text{ secs.}$$

References

1. H. Chang, Institute for Direct Energy Conversion, Univ. of Penna., "An Unsteady-state Method for Measuring Thermal Diffusivity of Solid Eutectic Mixtures of Refractory Materials at High Temperatures." Prepared for Research towards Ph.D. degree.

2. (a) J. A. Cape, W. Lehman, and M. M. Nakata, "Transient Thermal Diffusivity Technique for Refractory Solids," Journal of Applied Physics, Vol. 34, Number 12, December, 1963.

(b) E.S. Fitzsimmons, "Thermal Diffusivity of Refractory Oxides," Journal of American Ceramic Society, Vol. 33, 327, #11,1950.

(c) A.F. VanZee, and C. L. Babcock, "A Method for the Measurement of Thermal Diffusivity of Molten Glass," Journal of American Ceramic Society, Vol. 34, Number 8, August 1951.

(d) H.S. Levine, "An Unsteady state Method for Measuring Thermal Diffusivity at High Temperatures," ONR Tech. Report, Alfred University, June 13, 1950.

(e) W.B. Crandall and G.E. Potter, "High Temperature Thermal Diffusivity Furnaces and Techniques for Measurement," ONR Tech. Report, Alfred University, January 1, 1953.

(f) R.L. Rudkin, R.J. Jenkins, and W.J. Parker, "Thermal Diffusivity Measurements on Metals at High Temperatures," The Review of Scientific Instruments, Vol. 33, Number 1, January, 1962.

(g) P.H. Sidles and G.C. Danielson, "Thermal Diffusivity Measurements at High Temperatures," in Thermoelectricity, edited by P.H. Egli, John Wiley and Sons, Inc., New York, 1960, p.p. 270-288.

3. C.H.S. Carslaw and J.C. Jaeger, "Conduction of Heat in Solids," 2nd Edition, Oxford at the Clarendon Press.

4. A.B. Newman, "Heating and Cooling Rectangular and Cylindrical Solids," Industrial and Engineering Chemistry, Vol. 28, No. 5, 1936.

5. K.K. Kelly, "Data on Theoretical Metallurgy X, High Temperature Heat Content, Heat Capacity, and Entropy Data for Inorganic Compounds," U.S. Bureau of Mines Bulletin No. 476, p. 251, 1949.

6. W.D. Kingery, J. Franel, R.L. Coble, and T. Vasilos, "Thermal Conductivity, Data for Several Pure Oxide Materials Corrected to Zero Porosity," Journal of Ceramics Society, Vol. 37, Number 2, p.p. 107-110.

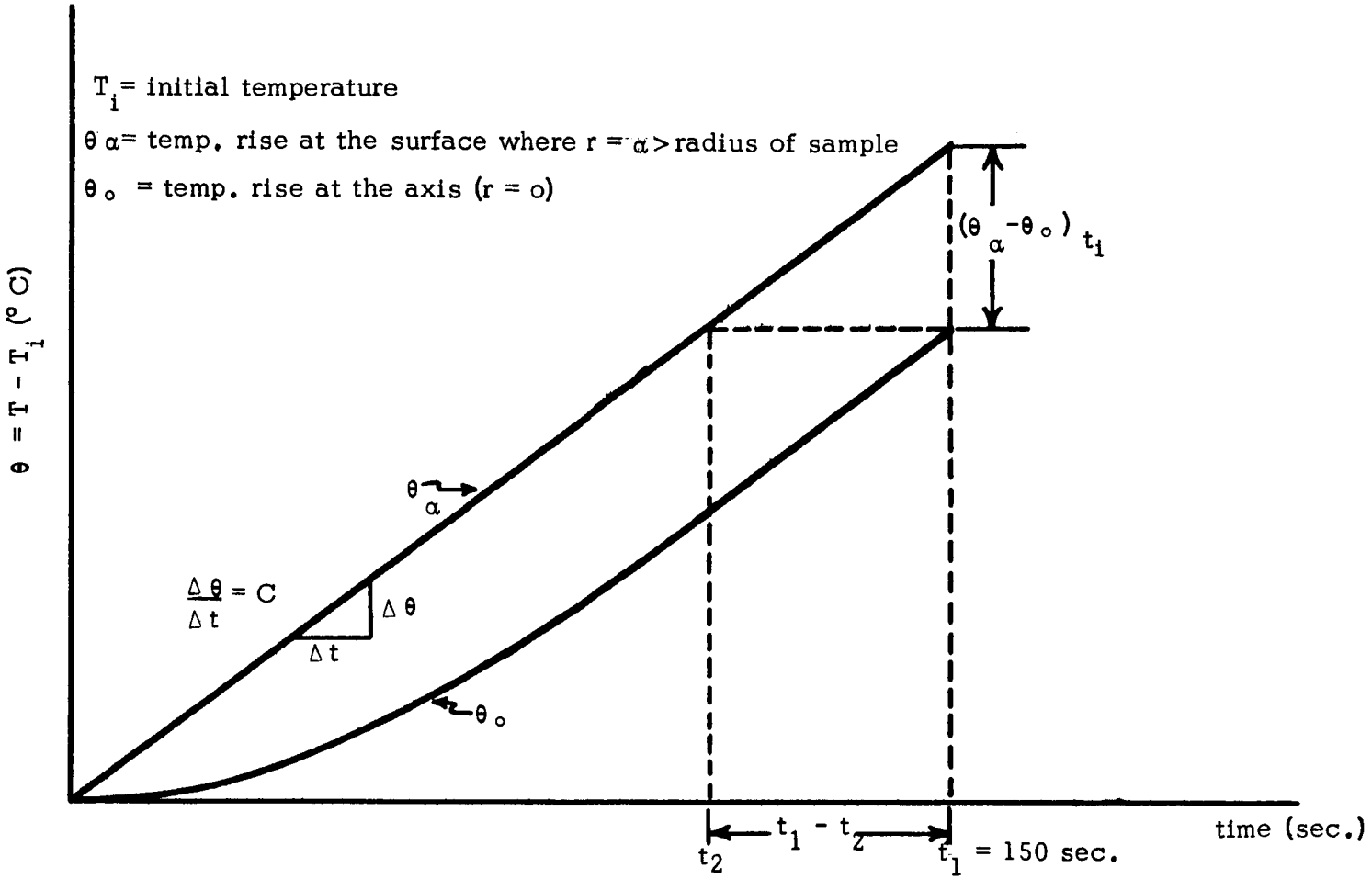

Figure 2.3-1. Temperature increase at surface and axis of sample.

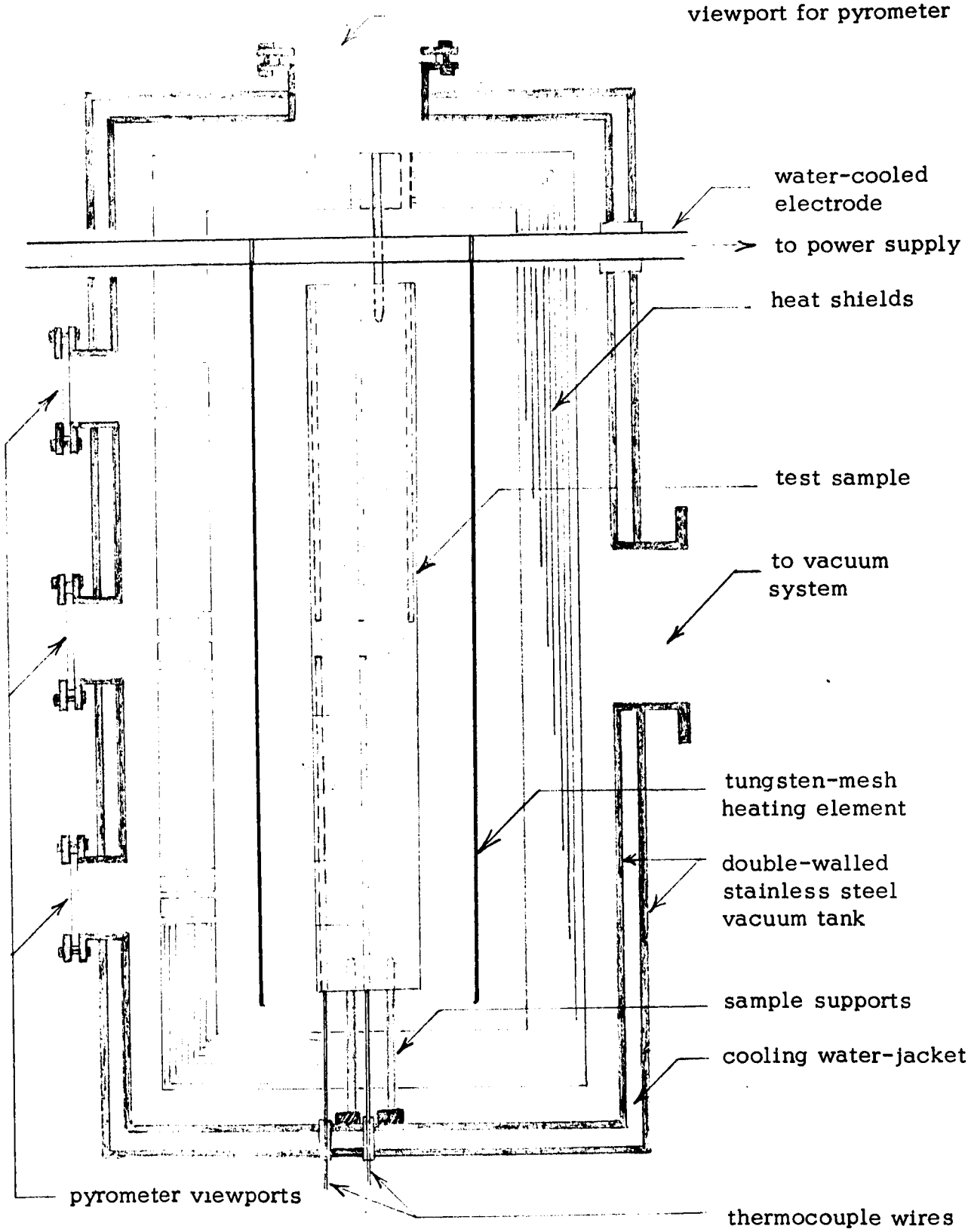

Figure 2.3-2 Vacuum furnace (side view)

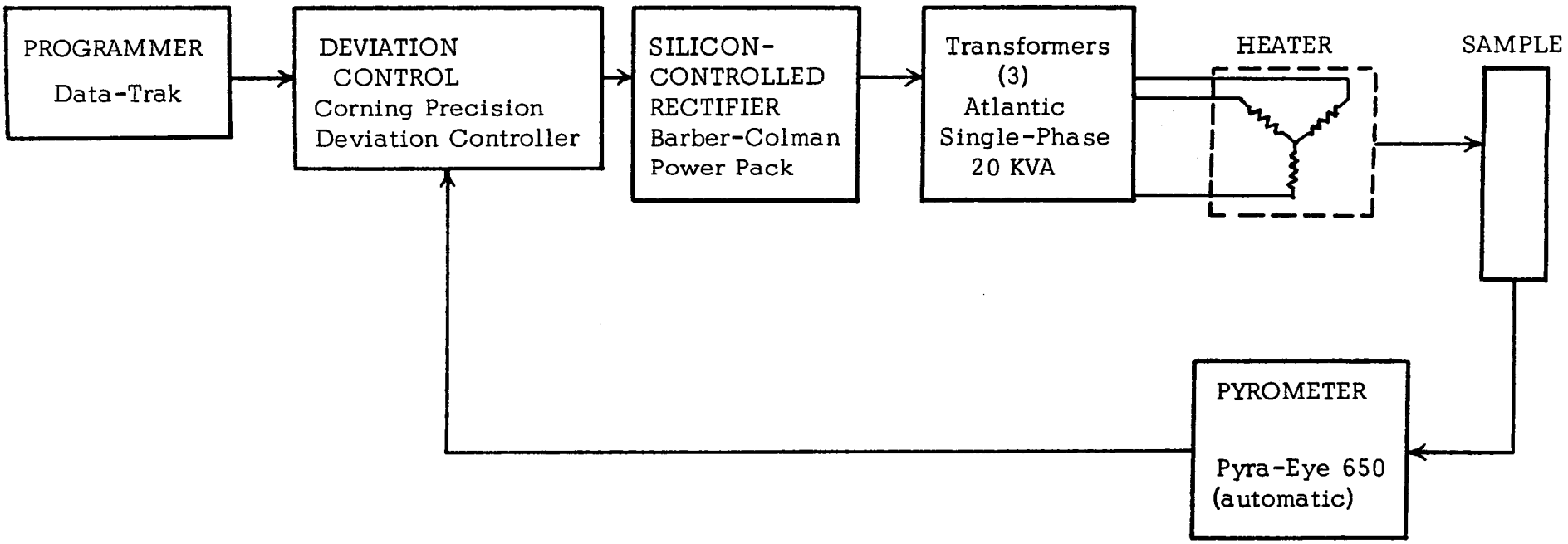

Fig. 2.3-3 Heater power supply and feed-back control system.

3. PLASMA ENGINEERING

Branch Chief: Dr. George L. Schrenk

Senior Members: Dr. Hsuan Yeh, Dr. Leon W. Zelby,

Dr. Chad F. Gottschlich

3.1 Emitter Surface Physics of Plasma Diodes

Dr. Leon W. Zelby, Dr. George L. Schrenk; M. Kaplit

The concept of a work function is an integral part of the theory of thermionic (plasma diode) energy converters. Researchers often use the term work function without specifying whether they mean the true, Richardson, effective, or some other type of work function. The classical definition of the work function is the energy difference between the Fermi level of the metal and the energy required to remove an electron from the Fermi level to infinity. By definition all these will give the correct value of electron emission; but the relationships between these various types of "work function" and the classical definition of "work function" is not clear. Clarification of this relationship is essential to an understanding of the various emission and adsorption processes in the plasma diode. Thus, as a first step to a more complete understanding of emission and adsorption phenomena, the significance and interrelationships of these various "work functions" have been studied theoretically.

The preliminary details of our findings are presented in Reference 1. The Richardson work function and its associated quantum mechanical electron reflection co-efficient were found to possess the most fundamental significance. This conclusion, however, required that the usage of the concept of a Richardson plot be examined and defined more precisely. The classical procedure for determining

the Richardson work function and the associated emission constant is through the use of Richardson plots.[3] Whereas this method is valid for emission in vacuum, the presence of a gaseous environment such as cesium vapor introduces another variable, surface coverage. The derivation of the Richardson equation is based on the assumption that the surface structure is independent of temperature. In gaseous environment this is only true at constant coverage. Consequently, Richardson plots are meaningful only at constant coverage.

Thus, the Richardson work function ϕ, measured at a constant surface coverage, is the minimum energy required to remove an electron from the Fermi level of the emitter to infinity.[4] Hence, the average energy that must be supplied to transfer an electron from the Fermi level of the emitter at temperature T to infinity is[5] $\phi + 2$ kT. Although this conclusion is in agreement with many thermionic pioneers, such as Herring and Nichols,[3] it is at variance with many present day thermionic researchers who claim that the effective work function is an empirical constant possessing no physical significance.[1]

This investigation of the significance and interrelationships of the various "work functions" has led to the development of a new macroscopic model of electron emission from metals in cesium environment. This model which requires no adjustable constants, includes

the concepts of the state of maximum activity and its relationship to the Richardson work function. Electron emission S - curves calculated on the basis of this model for a cesium-tungsten system show excellent agreement over more than seven orders of magnitude of the cesium arrival rate with the experiments of Houston[6] and Langmuir and Kingdon.[7] Preliminary parts of this theory are presented in Reference 1, details in Reference 2. Figure 3.1-1 shows a set of electron emission S - curves, as obtained from this theory, compared with Houston's experiments.

As discussed in the previous progress report, the primary problem under investigation is the calculation of the surface charge distribution at a metal-vapor interface. However before this microscopic problem could be solved to the extent desired, it was necessary that a good macroscopic theory exist and that a clear understanding of the interrelationships between the various types of "work functions" exist. A detailed literature survey showed that these needs were not met by present work; hence the research described above was carried out prior to calculation of the surface charge distribution at a metal-vapor interface.

The central purpose of this research is to predict the surface charge as a function of the crystallographic structure of the substrate, the number of adsorbed particles, and the fraction of charge associated with the ionic and covalent bonding between the

adsorbed particles and the substrate. Because we desire to explicitly include the effects of coverage and substrate structure, a three-dimensional solution is necessary. Of the methods presently available (plasma oscillation theory, Hartree-Fock, etc.), statistical theory appears to be the only one for which a three-dimensional solution is analytically feasible. We shall now outline this method.

The fundamental idea of the statistical method is to work with the particle density rather than with the quantum mechanical wave function when solving many-body problems.[8] To solve such a problem, one determines the total energy of the system in terms of the particle density, which contains a number of adjustable constants. These constants can be evaluated by using the fact that the total energy of the system must be a minimum at surface coverage equilibrium.

The total energy consists of many parts. The first is a kinetic energy, KE, which in terms of the particle density, n, is

$$KE = \int \left(A n^{5/3} + B \frac{|\nabla n|^2}{n} \right) d\vec{r}$$

where A, B are constants. The first term of the integrand is the Thomas-Fermi energy and the second the Weiszacker energy. A good discussion of these can be found in the article by March and Young.[9]

The potential energy of this system is more difficult to obtain. First, there are those contributions due to the hard-core atoms, i.e., their mutual electrostatic interactions and those with the surrounding electron gas. Let us call these two potential energies V_{hc-hc} and V_{hc-e}, respectively. The next potential energy is the electrostatic energy of the electron gas, V_{ee}, which is obtained from

$$V_{ee} = \int \frac{e^2 n(\vec{r}_1)\, n(\vec{r}_2)}{4\pi\epsilon_0 |\vec{r}_1 - \vec{r}_2|}\, d\vec{r}_1\, d\vec{r}_2$$

The final two potential energy terms are quantum mechanical in origin. They are due to the mutual repulsions of the electrons arising from the Pauli principle and from electrostatic forces. These two energies are extremely difficult to determine exactly and we shall employ the free electron approximations which have led to meaningful results in calculating the cohesive energy and the surface double layer of sodium.[10] The first is the exchange energy V_{er} and the second the correlation energy V_{cor}.[11]

$$V_{er} \propto -\int n^{4/3}\, d\vec{r}$$

$$V_{cor} \propto -\int \frac{n}{5.51 + \left(\frac{3}{4\pi n}\right)^{1/3}}\, d\vec{r}$$

These approximations are equivalent to assuming a locally uniform particle density.

The total energy is then the sum of the above

$$E = KE + V_{hc-hc} + V_{hc-e} + V_{ee} + V_{er} + V_{cor}$$

To actually calculate $E = E(n)$ is rather involved and the details for doing this so as to include the effects of substrate geometry, chemical bonding, and coverage will be presented in Reference 12.

Research work is currently proceeding on the analytic evaluation of the various terms that contribute to the total energy and on the development of numerical techniques for minimizing the total energy.

References

1. M. Kaplit, G. Schrenk, L. Zelby, "Electron Emission from Metals in Gaseous Environment," Thermionic Specialist Conference Proceedings, Cleveland, Ohio, Oct. 26-28, 1964.
2. M. Kaplit, G. Schrenk, L. Zelby, "Macroscopic Theory of Electron Emission from Metals in Gaseous Environment," Article in preparation.
3. C. Herring and M.H. Nichols, "Thermionic Emission," Reviews of Modern Physics, Vol. 21, No. 2, pp. 185-270, April 1949.
4. R. Fowler and E.A. Guggenheim, "Statistical Thermodynamics," Cambridge at the University Press, 1960, Chapter XI.
   R. Fowler, "Statistical Mechanics," Cambridge at the University Press, 1955, second edition, chapter XI.
5. Dekker, "Solid State Physics," Prentice Hall, 1957.

6. J.M. Houston and H.F. Webster, "Advances in Electronics and Electron Physics," (Academic Press, New York, 1962), vol. 17, p. 125.

7. I. Langmuir and K.H. Kingdon, Proc. Royal Soc. A(London), 107 61 (1925).

8. N.H. March, "The Thomas-Fermi Approximation in Quantum Mechanics," Advances in Physics, 6, 1-101 (1957).

9. N.H. March and W.H. Young, "Variational Methods Based on the Density Matrix," Proc. of the Phys. Soc. A., 71, 182-192 (1958).

10. E. Wigner and J. Bardeen, "Theory of the Work Functions of Monovalent Metals," Phys. Rev., vol. 48, pp. 84-87, 1935. J. Bardeen, "Theory of the Work Function, II; The Surface Double Layer," Phys. Rev., vol. 49, pp. 653-663, 1936.

11. F. Seitz, "Modern Theory of Solids (McGraw-Hill Book Co., New York, 1940).

12. M. Kaplit, Ph.D. Dissertation, University of Pennsylvania

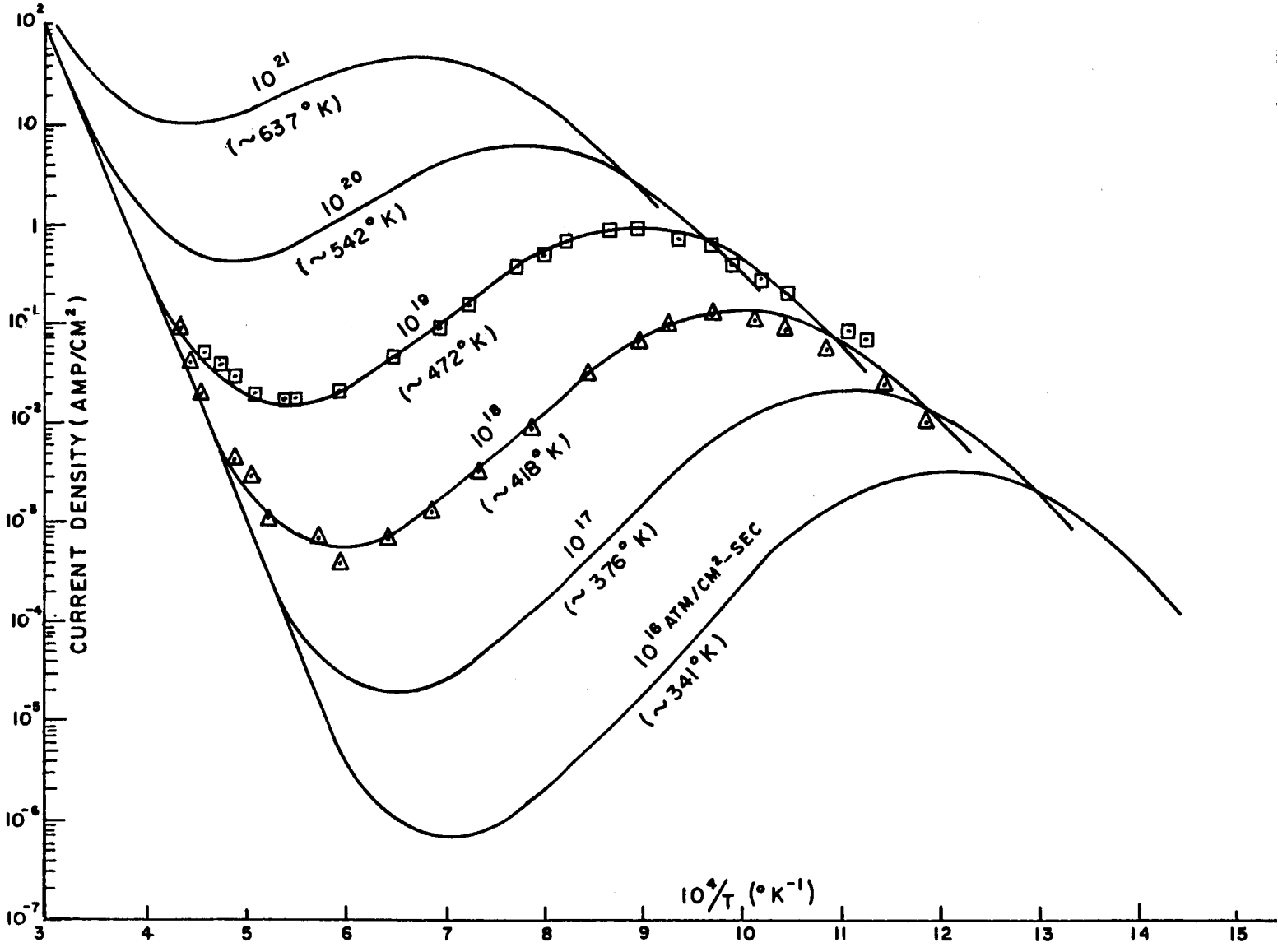

Fig. 3.1-1. Theoretical electron emission S curves for a cesium-tungsten system compared with Houston's data.[6]

3.2 Emitter Sheath Polarity in Plasma Diodes

Dr. George L. Schrenk

The general criteria used to determine the sign (polarity) of the emitter sheath in a plasma diode have been examined in detail. The criteria presently in use in both close- and broad-spaced cesium plasma diodes are

$I_s/I_{pE} > 491 \Rightarrow$ electron rich (negative) emitter sheath,

$I_s/I_{pE} < 491 \Rightarrow$ ion rich (positive) emitter sheath,

where I_s is the electron emission current (as given by the Richardson equation) and I_{pE} is the ion current from the emitter. It has been shown[3,4] that these criteria follow directly from a more general set of criteria by assuming that no collisions occur in the interelectrode space. Thus, the applicability of these criteria to a close-spaced collisionless diode cannot be questioned.

In a broad-spaced plasma diode, however, there are interactions in the interelectrode space and these interactions give rise to volume ionization and/or recombination. Since the presence of volume ionization in the interelectrode space of a plasma diode affects the potential distribution, it must also enter into the determination of the emitter sheath polarity. The criteria stated above, however, do not take into account such effects.

A phenomenological macroscopic model has been used to determine the

correct criteria when interactions exist in the interelectrode space. Specifically, this model applies to a broad-spaced plasma diode where the spacing is many times the mean free path -- i.e., to the case where a plasma, characterized by its own variables, is formed in the interelectrode space. No specific mechanism and rates for volume ionization and/or recombination were assumed; both the net volume ionization and the plasma electron temperature are treated as unknown parameters. The basic assumptions used in this model are:

1. The temperature of the collector is low so that electron and ion generation at the collector are negligible.

2. The Saha-Langmuir equation is a valid representation of ion generation at the emitter surface. This equation, however, has been rewritten so as to use the electron emission current I_{so} explicitly. This means that the concept of an emitter work function is never explicitly introduced.

3. The plasma in the interelectrode space is uniform with the ion density equal to the electron density throughout.

4. Maxwellian distributions of electrons and ions exist in the plasma; the corresponding electron and gas temperatures, however, need not be equal.

5. Plasma resistance has been neglected.

6. Extraneous losses, such as thermal radiation from the plasma to the surroundings, loss of electrons, ions, and atoms from the interelectrode space are neglected.

7. Only two species of cesium are considered to exist in the plasma, i.e. atoms and ions. No provisions are presently made for the possible existence of excited atoms and/or molecules.

Using these assumptions, a set of six simultaneous equations has been formulated to describe the condition when the emitter sheath vanishes. Although a detailed derivation of this set of six equations will not be presented here (see Ref. 4), a brief discussion of each equation follows:

For the current balance at the emitter surface, the net current I is the result of four groups of charge carriers: (1) saturation current from the emitter I_{so}; (2) ion current from the emitter I_{pE}; (3) electrons from the plasma (reverse electron current) I_{ep}; and (4) ions from the plasma (reverse ion current) I_p.

Thus $$I = I_{so} - I_{pE} + I_p - I_{ep}.$$

For the current balance at the collector surface, the net current I is the result of only two groups of charge carriers: (1) electrons from the plasma $I_{ep} \exp(-V_{SC}/V_{Te})$; and (2) ions from the plasma I_p, where V_{Te} denotes the electron plasma temperature. The collector

sheath is always assumed to be positive in this model. Thus

$$I = I_{ep} \exp (V_{SC}/V_{Te}) - I_p.$$

The equation for the ion balance across the plasma is

$$I_{pE} + A_{DE} = 2I_p,$$

where A_{DE} is the net volume ionization and/or recombination in amps/cm^2.

The equation for the ion production at the emitter is

$$I_{pE} = I_a / [1 + 2I_{so} \exp (V_i / V_{TE}) A T_E^2]$$

where I_a = arrival rate of atoms and ions from the plasma,

V_i = ionization potential of cesium,

V_{TE} = emitter temperature (ev),

A = thermionic emission constant (120 amps/cm^2).

This is the Saha-Langmuir equation, rederived in a manner such that the concept of an emitter work function is never explicitly introduced.

The equation for the charge density balance in the plasma is

$$I_{ep} \sqrt{m_e / V_{Te}} = I_p \sqrt{m_p / V_G}$$

where V_G denotes the gas temperature (ev).

The equation for the energy balance for the plasma is

$$2 I_{so} (V_{TE} - V_{TE}) + 2 I_a (V_{TE} + V_{TC} - 2 V_G)$$
$$- A_{DE} (V_i + 2 V_{Te}) - (I + I_p) V_{SC} = 0,$$

where V_{TC} is the collector temperature (ev). Although the approach used to obtain this equation is similar to that employed in Reference 1, the reference points and grouping of terms used are fundamentally and significantly different. This equation expresses the fact that the net energy flowing across a similar imaginary surface immediately outside the collector when the same potential reference points are used for both imaginary surfaces. Since only ions and atoms are considered to be crossing these imaginary surfaces, the possible presence of excited atoms and/or molecules has been neglected.

Special numerical procedures have been developed to solve these six simultaneous non-linear coupled equations without introducing any additional numerical approximations. The input variables are T_E, T_C, T_G and I_a. For each value of A_{DE} and V_{Te} chosen, a numerical search is carried out to find a solution of these equations in terms of I_{so}. Such a solution may or may not be found. If a solution is found, it means that for the values of T_E, T_C, T_G, I_a, A_{DE} and V_{Te} chosen, a zero emitter sheath solution exists for the value of I_{so} found. If no solution is found, no zero emitter sheath can exist for the conditions chosen.

Since A_{DE} and V_{Te} are treated as independent variables, the solutions found for each set of values of T_E, T_C, T_G, and I_a will be a family of curves on a plot of I_s versus A_{DE}. Each curve in this family can be labeled with a value of V_{Te}. Physical conditions on this set of equations (e.g., $I_p \geq 0$, etc.) restrict this family of curves to a specific region of the I_s - A_{DE} plane.

As a first step in the solution of this set of equations, it is convenient to find the envelope of this family of curves. An analytical procedure has been found for solving these equations for this envelope. Figure 3.2-1 shows a typical envelope for $0 \geq V_{Te} \geq \infty$ with the various significant features labeled. The two lines extending to the right meet at infinity. The limits $0 \geq V_{Te} \geq \infty$ arise from the use of V_{Te} as a mathematical parameter in the analytical solution. All solutions for I_{so} as a function of A_{DE} and V_{Te} lie within the boundaries of this envelope.

Physically, it is clear that $V_{Te} \geq V_G$. The inclusion of this fact, however, is not simple. A solution for the envelope with the restriction $V_{Te} \geq V_G$ yields a portion of the envelope in Figure 3.2-1; but this portion is not closed. To find the full envelope it is necessary to solve for the solution for $V_{Te} = V_G$. This has been done and the results are shown in Figure 3.2-2.

Any broad-spaced plasma diode operating above the top curve in

Figure 3.2-2 necessarily possesses an electron rich (negative) emitter sheath. Any broad-spaced plasma diode operating below the bottom curve in Figure 3.2-2 necessarily possesses an ion rich (positive) emitter sheath. From this figure it is clear that an increase in the net volume ionization with all other parameters constant can cause the operation of such a plasma diode to go from an electron rich to an ion rich emitter sheath.

For plasma diodes operating in the region between the two curves in Figure 3.2-2, it is impossible to state whether the emitter sheath is positive or negative without having more information. First, the entire parametric family of curves ($\infty \geq V_{Te} \geq V_G$) is needed for the region bounded by this envelope. Analytical procedures have been developed for solving these equations for the full parametric family of curves (Ref. 4). One typical family is shown in Figure 3.2-3. This family, however, is still not sufficient to uniquely define the polarity of the sheath; it is still necessary to obtain the specific solution that relates A_{DE} to V_{Te}. Only after this precise curve has been specified can conclusions be drawn about the polarity of emitter sheaths for plasma diodes operating in the region between the two envelopes in these figures.

The results in Figure 3.2-3 are not in the most convenient form for use in the interpretation of current-voltage characteristics. These results are given in terms of I_s while experimental measurements

yield I. The precise determination of I_s from I is very difficult, if not impossible, in broad-spaced plasma diodes. Thus, it is desirable to develop criteria in terms of I. This has been done and a typical result is shown in Figure 3.2-4. It will be noticed that the lower envelope is in the ion current region. A study of this figure shows that the reverse current can be a useful diagnostic tool in determining the polarity of the emitter sheath; if the magnitude of the reverse current is large enough, the emitter sheath is ion rich. Knowledge of the emitter sheath polarity is a necessary requisite to any analysis of the potential distribution in the interelectrode space.

A number of results obtained from this model are presented in Reference 4. Since the current-voltage characteristics of a plasma diode depend rather sensitively on the sign of the emitter sheath, these results are useful in correlating theoretical and experimental results from plasma diode energy converters. Such a correlation will initially consist of a study of the conditions under which a transition to the ignited mode occurs in the current-voltage curves. The intercept of the current at the transition point with the envelope of the family of zero sheath solutions yields bounds to the average net volume ionization. A knowledge of the electron temperature at the transition point is required to determine a definite average net volume ionization. Once the average net volume

ionization is known at one spacing, it is possible to predict the variation of the ignited mode transition point with spacing for braod-spaced diodes. As more experimental information is obtained from plasma diodes operating in various modes, each point in the operation of a diode, including hysteresis current-voltage effects, can be represented by some point on one of these plots. These plots can then be to plasma diode energy conversion what phase diagrams are to physical chemistry.

References

1. Talaat, M.E., "The Surface Ionization and Volume Ionization Modes of Operation in the Thermionic Plasma Energy Converter," Advanced Energy Conversion, Vol. 2, (1962), pp. 447-458.
   Talaat, M.E., "Generalized Theory of the Thermionic Energy Converter," AIEE General Meeting, New York, Jan. 28 - Feb. 2, 1962. Paper No. 62-291.
2. Dunlop, J. and Schrenk, G., "Theoretical Model of a Thermionic Converter," Proceedings of the Thermionic Conversion Specialist Conference, Oct. 7-9, 1963, pp. 57-62.
3. Schrenk, G. L., "Emitter Sheath Polarity In Plasma Diodes," Proceedings of the Thermionic Conversion Specialist Conference, Cleveland, Ohio, Oct. 26-28, 1964.
4. Schrenk, G. L., "Criteria For Emitter Sheath Polarity In Plasma Diodes," ASME Winter Annual Meeting, New York, Nov. 29 - Dec. 3, 1964.

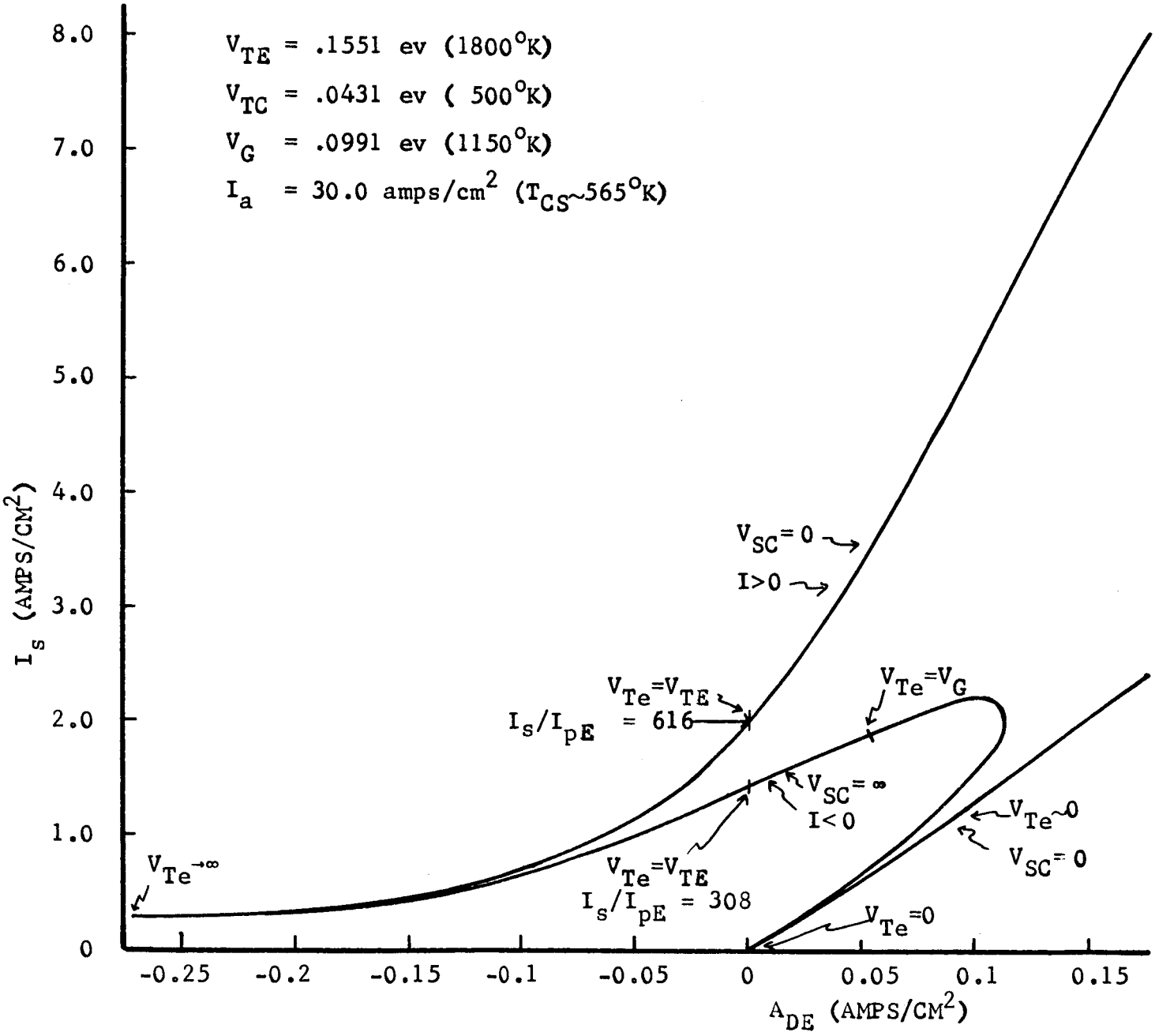

Figure 3.2-1 Envelope of zero emitter sheath solutions for $0 < V_{Te} < \infty$.

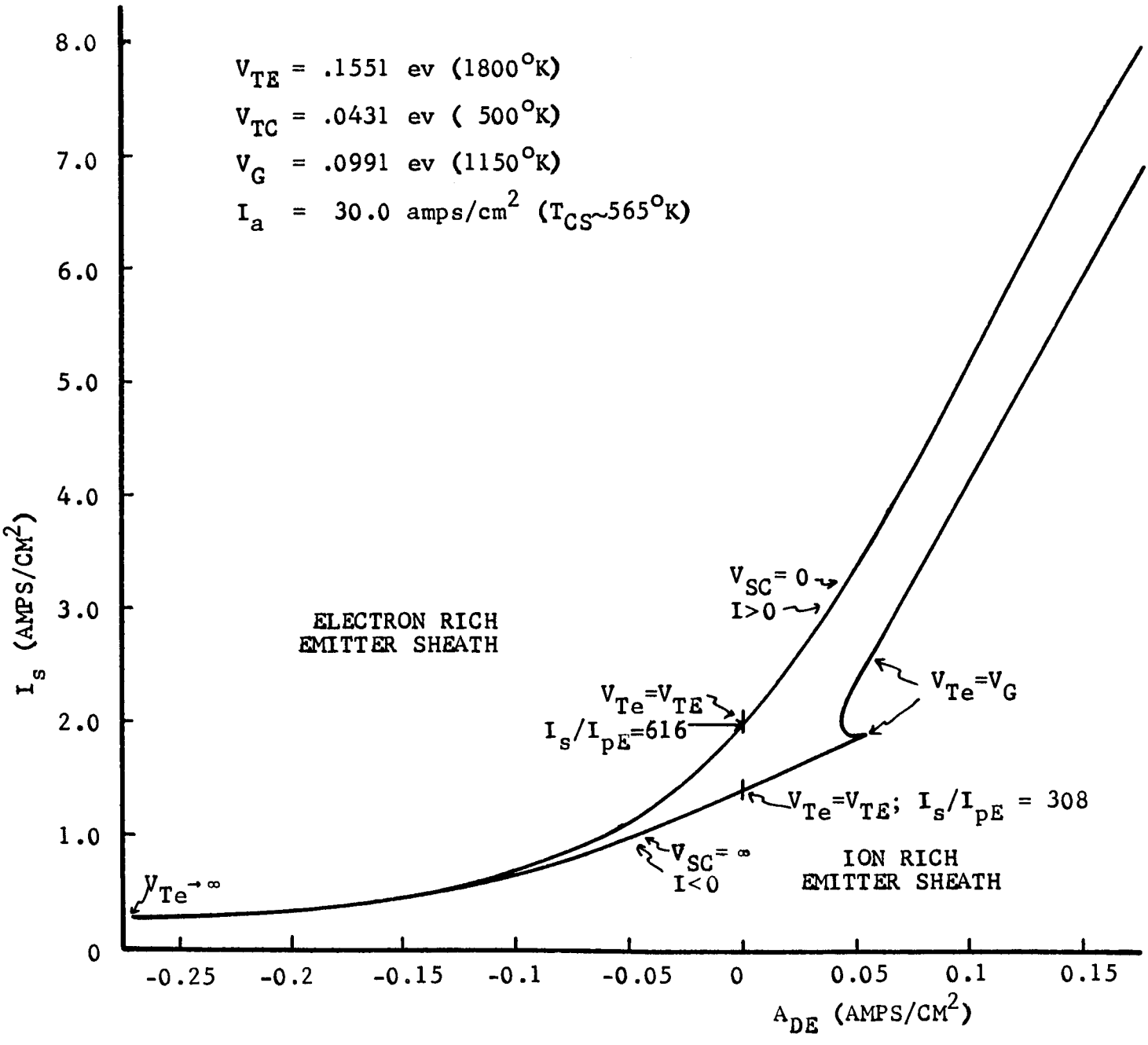

Figure 3.2-2 Envelope of zero emitter sheath solutions for $V_G < V_{Te} < \infty$.

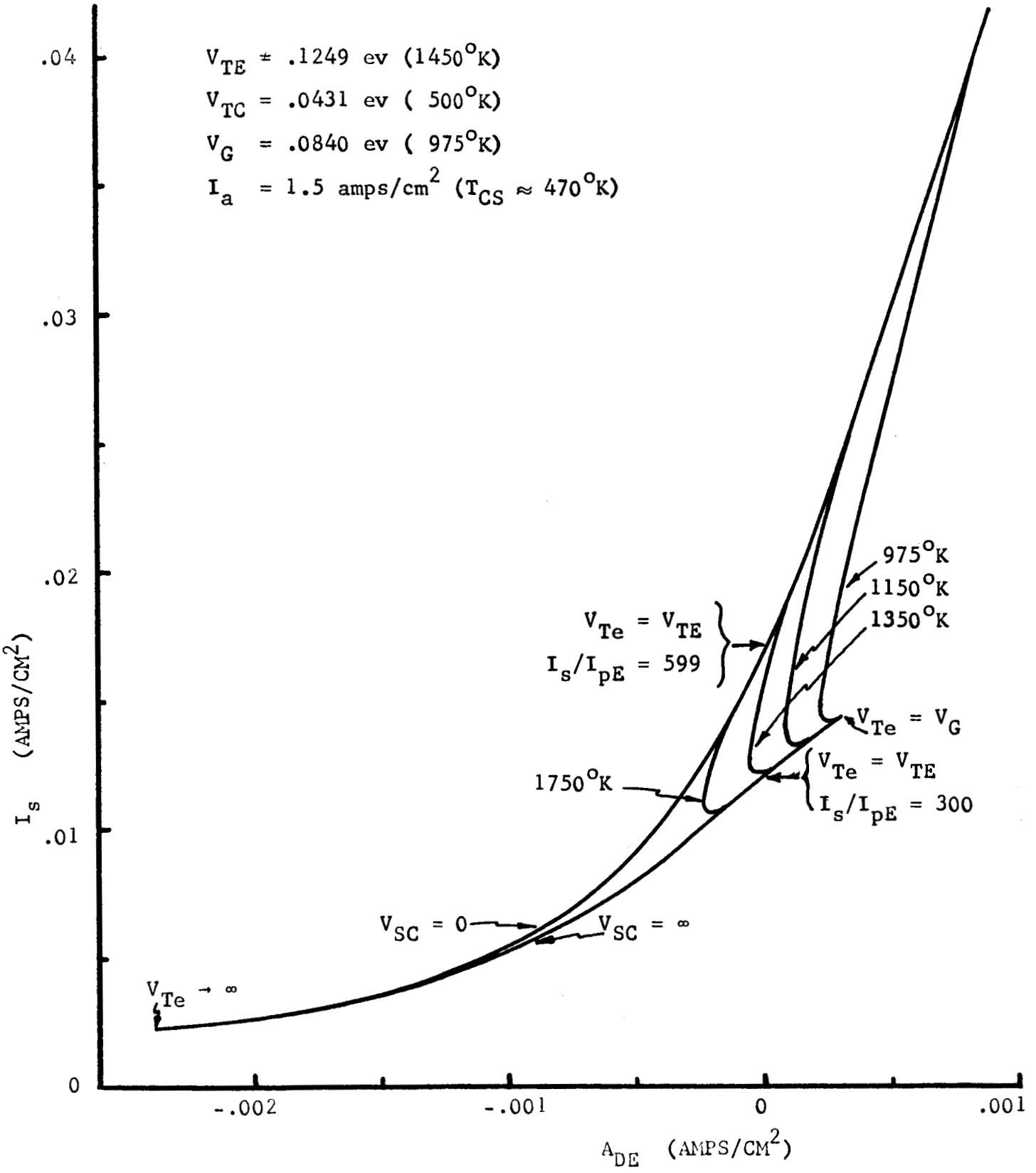

Figure 3.2-3. Family of zero emitter sheath solutions in terms of I_s

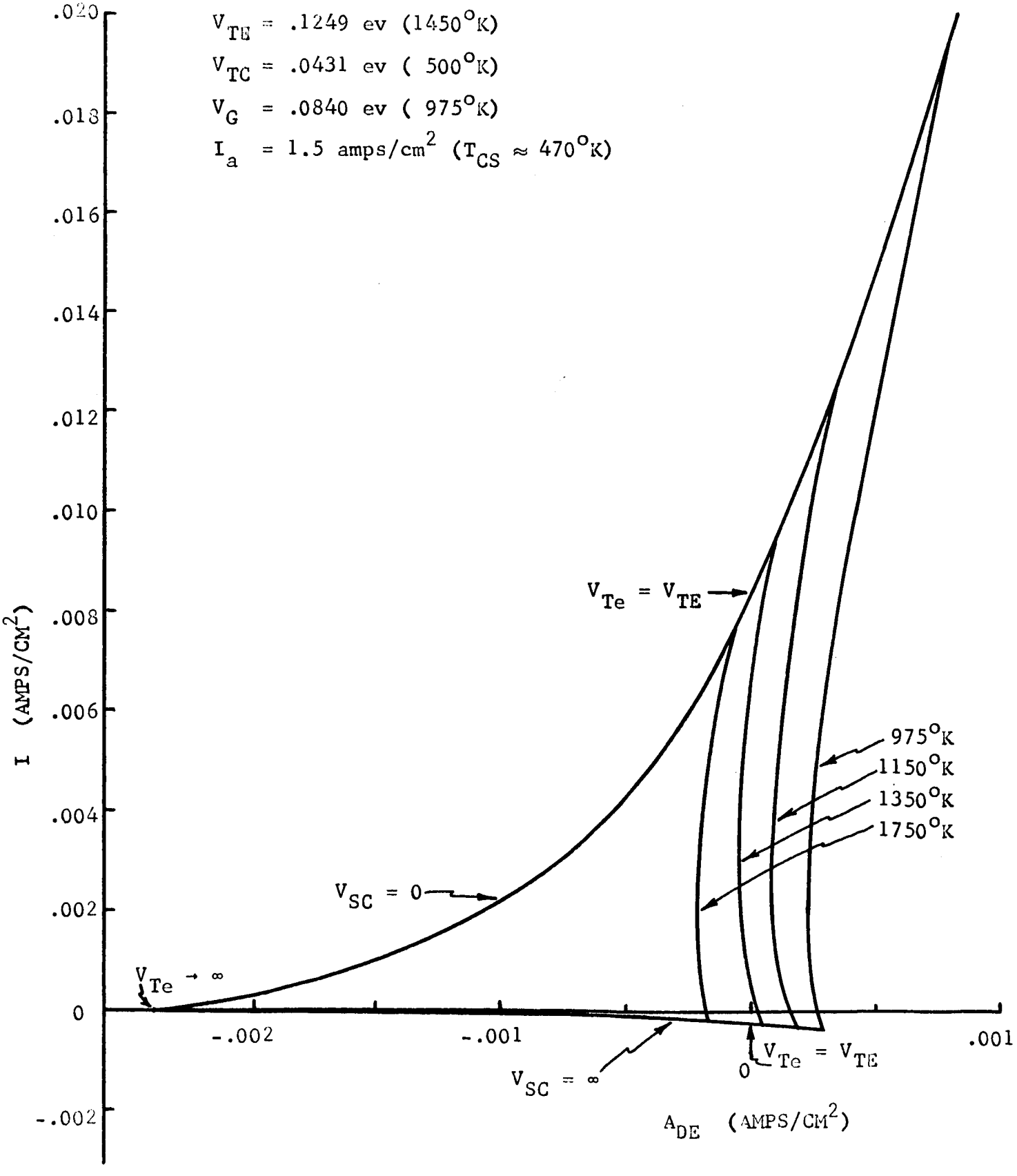

Figure 3.2-4. Family of zero emitter sheath solutions in terms of I.

3.3 Investigation of Na-K Seeded Argon Plasma

Dr. Hsuan Yeh, Dr. Chad F. Gottschlich; T. K. Chu

The research reported here is a continuation of efforts discussed in previous progress reports. The objective of this work is to measure non-equilibrium ionization and its effects in an alkali metal (Na-K) seeded argon plasma, where the non-equilibrium ionization is produced by an externally applied electric field. Measurements of the electric field, plasma current, and spectrophotometric measurements of the radiation from the plasma will be made. These spectrophotometric measurements are especially significant because, by proper interpretation, the radiation yields information on the local properties of the plasma -- e.g., the electron and atom-ion spatial temperature distributions, etc. From these spectrophotometric measurements, electrical measurements, and separate measurements of the pressure and chemical composition of the plasma, we will be able to calculate the local values of the electrical conductivity, thermal conductivity and specific radiation.

Recent efforts have been largely devoted to improvement of the Na-K alloy injection system. Reliable and precise control of the volume flow rate of the alloy has been accomplished by a motor-driven, variable-gear drive (see Fig. 3.3-1) in conjunction with a syringe. The syringe cylinder is made from Pyrex tubing and the piston is made of polyethylene. This design very effectively eliminates the

leakage of alloy between the cylinder and piston that occurred in earlier designs.

A new alloy boiler to vaporize the alloy to be mixed with the argon has been constructed and tested (see Fig. 3.3-2). In the new system the liquid alloy is sprayed into a stream of hot argon (600°C). This argon has been heated by passing through a stainless steel coil which is externally heated. The two-phase mixture of argon and Na-K alloy then passes through a four-turn stainless steel coil of 0.436" - I.D. and with a total length of 11 feet. The coil is situated in a muffle furnace maintained at 850°C. The alloy completely vaporizes in the coil. The coil is adequately sized so that the alloy-argon vapor mixture leaves at a temperature of 650°C, well above the dew point of the mixture (approximately 420°C for 1% concentration of alloy).

Materials difficulties with the mixing chamber have been eliminated by using a nitrogen cooled, stainless steel chamber as shown in Fig. 3.3-3. It was found that six radial distribution ports 0.141 inches in diameter were necessary for good mixing between the alloy-argon stream mentioned above and a high-temperature stream of argon from a plasma-arc jet. The second argon stream is used to control the temperature of the final mixture.

Recent tests have shown that the quartz test section rapidly

devitrifies during operation. This appears to be due to traces of oxygen and water vapor present in the argon. It is known that oxygen and water vapor can react with Na-K alloy to form oxides that, in turn, can react with quartz. Hence, we are constructing a gas purification system using 1/8" pellets of Linde 4Å molecular sieve material and 1/4" to 1/8" lumps of manganous oxide in columns to remove the water and oxygen, respectively. It is anticipated that elimination of water and oxygen should eliminate devitrification.

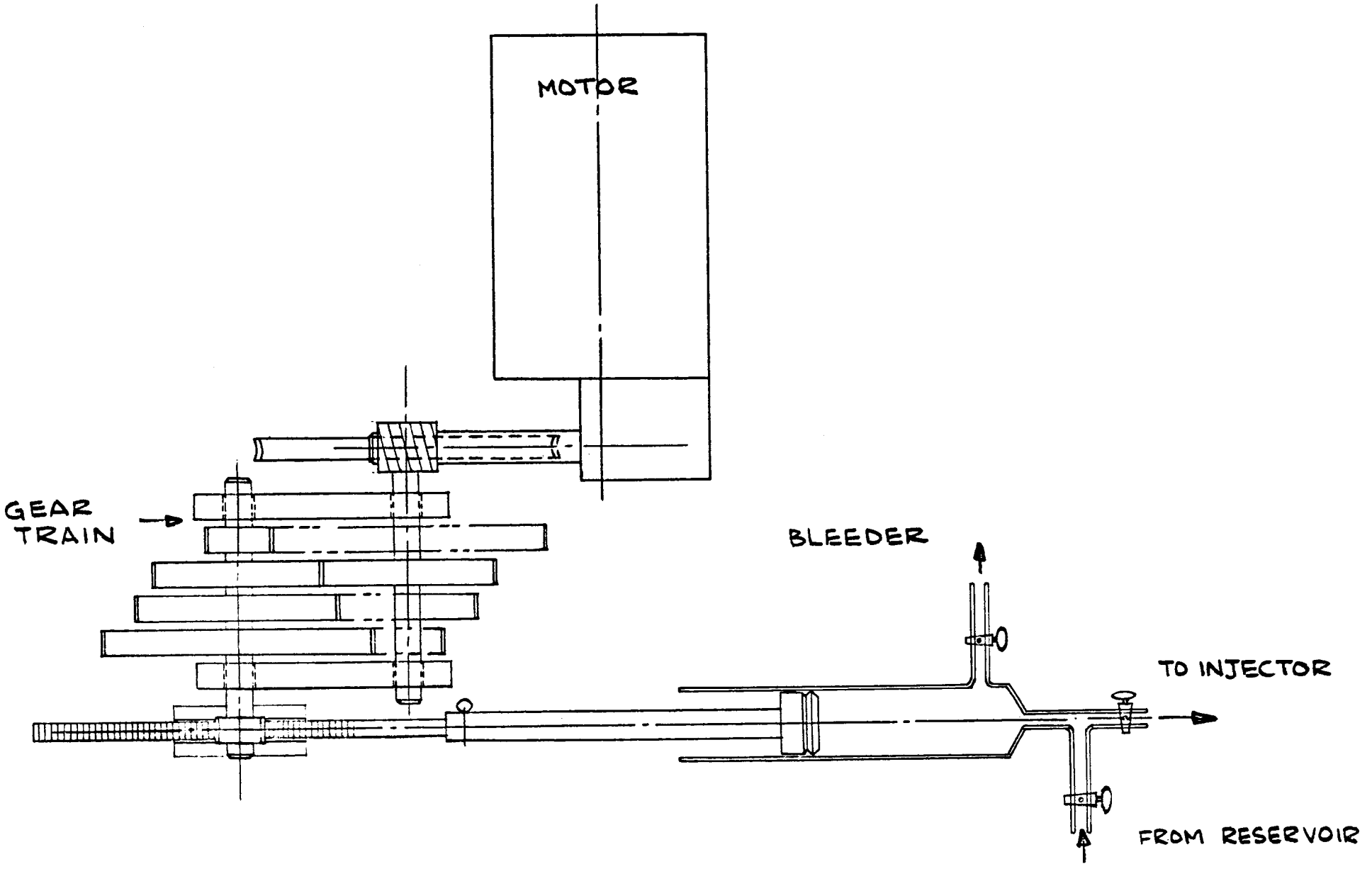

Figure 3.3-1. Motor-driven syringe.

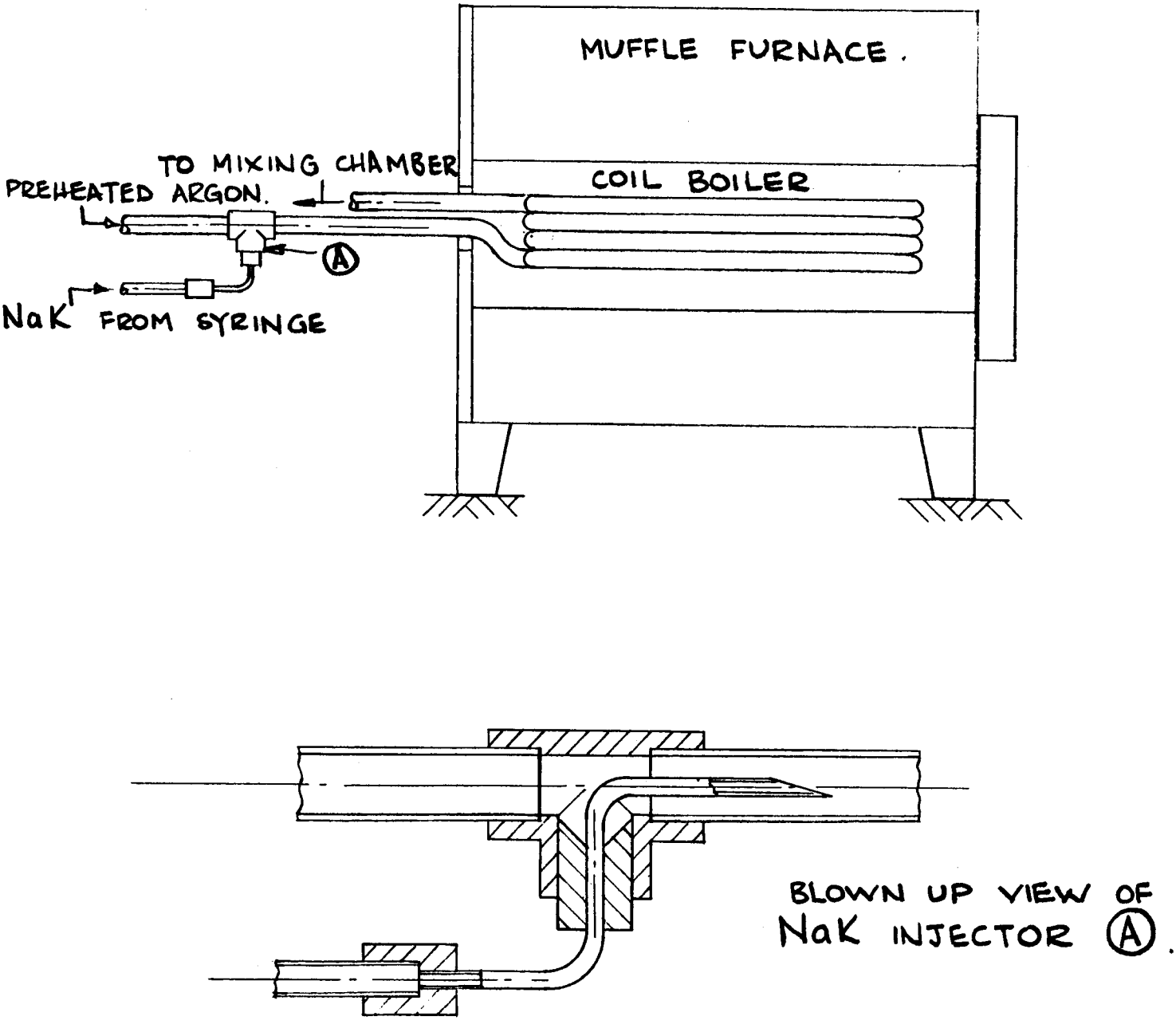

Figure 3.3-2. Alloy boiler.

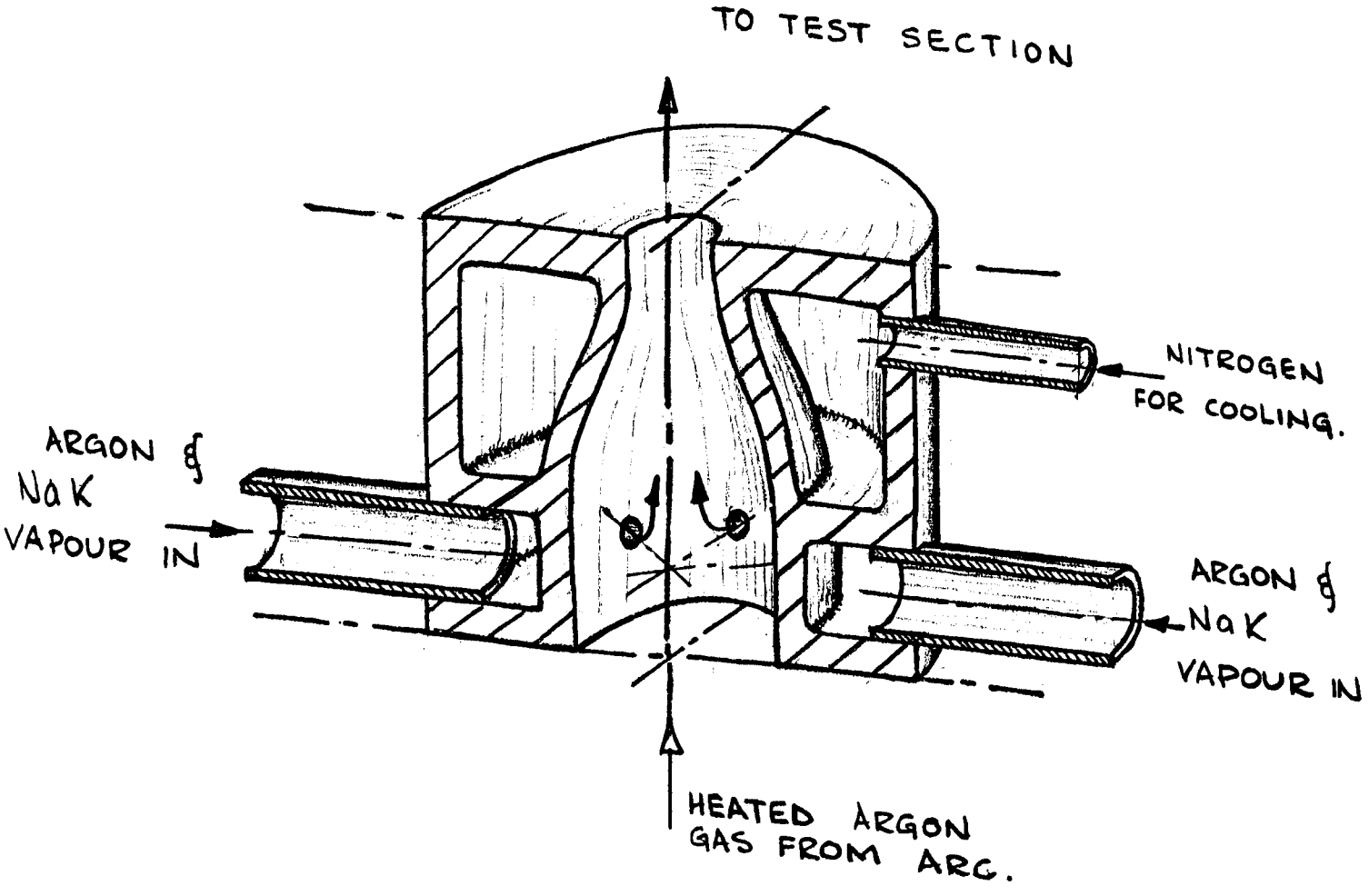

Figure 3.3-3. Nitrogen cooled stainless steel mixing chamber.

4. ELECTROCHEMICAL ENGINEERING

Branch Chief: Dr. Leonard Nanis

N65 19783

4.1 Transient Concentration Variation in Natural Convection Electrolysis

Dr. Leonard Nanis

Expansion of the Institute activities in the area of electrochemical engineering will permit investigation of topics of general interest to fuel cell development and research, in addition to previous work directed towards the biological fuel cell. The present state of the art of fuel cells suggests that concentrations of effort leading to the development of rational engineering design criteria are necessary and desirable. The commonly used porous electrode is particularly in need of study from the viewpoints of predictive model development and possible radically different synthetic constructional methods based on model studies.

In order to probe directly into the mass transport characteristics of an actual pore or representative model system, methods must be developed for measuring local transport rates on a micro scale. The well known technique of utilizing measured limiting current densities of cathodic reactions for evaluation of the mass transport boundary layer thickness can, of course, be applied to pore models such as an electrolyte meniscus on a plate electrode. However, this method is time consuming since the entire current density-overpotential curve must be obtained. Also, depletion effects are troublesome in the confined geometry of an actual pore model,

e.g., depletion of dissolved hydrogen by anodic oxidation at a platinized platinum pore surface. The present study is an attempt to develop a rapid method to be used in combination with micro probes located within a model pore region. The fundamental parameter sought is the thickness of the electrolyte layer which becomes depleted of dissolved electroactive species, for constant local current density operation.

The analysis of the transient behavior of electrode-electrolyte interface concentration (for a current step) will be combined with a relation between concentration and overpotential so that polarization transients will be predictable for assumed values of boundary layer thickness.

It is expected that only natural convection conditions will prevail in electrode pores. As will be shown, the behavior of the concentration transient at the interface is independent of actual convection conditions during a considerable portion of the transient. This finding, in combination with the potential-concentration relation will permit assessment of mass transport behavior for pore geometries which, by their nature, lead to considerable mathematical difficulty for exact convection analysis, e.g., thin films of electrolyte and curved meniscus regions.

Transient phenomena for transport processes have received renewed

attention recently, both theoretically and experimentally, particularly for heat transfer.[1,2] The usual method of treatment is based on a solution of the combined Navier-Stokes equations, continuity equation and diffusion equation with generalized convective terms. The difficulties associated with the solution of the resulting non-linear equations are well known. In the present development, for vertical plates, the overall complexity may be avoided by consideration of physically extreme cases in combination with general behavior of boundary layers. Although the development has been prompted by a purely electrochemical example, general applicability prevails.

The concentration changes at electrodes arising from the passage of constant current can be described for physical extremes which bound all real cases of natural convection self-stirring produced by density changes in a boundary layer which is being established i.e. in a transient condition. The heat transfer analog pertains to a sudden step in heat flux at a vertical plate of negligible thickness.

Following the switching on of a constant current in an electrolytic system, the complex interplay of ionic migration, diffusion and convection fluxes controls the time variation of the concentration in a region immediately adjacent to the electrode (anode or cathode). Ultimately, a steady state condition is attained where

the concentration contour is stabilized within a boundary layer region. In the heat transfer case, there is no direct analog of the field dependent electrolytic transport of migration of charged species. However, liquid density differences caused by the temperature variation in the boundary layer are analogous to the density differences induced by concentration changes in electrolysis. For convenience, the extreme cases are designated "Diffusion" and "Combined Diffusion and Convection."

Diffusion

The case where diffusional flux alone is present (as for a horizontal cathode facing downward) was worked out for one dimensional diffusion with constant gradient (constant current density) at the electrode by Weber[3] in 1879 and Sand[4] in 1901. The space-time variation of concentration is given for the cathode, as

$$C_{x,t} = C_b - \frac{J}{ZFD}\left[\frac{2D^{1/2}t^{1/2}}{\pi^{1/2}}\, e^{-\frac{x^2}{4Dt}} + x\ \mathrm{erfc}\ \frac{x}{2D^{1/2}t^{1/2}}\right] \quad (4.1\text{-}1)$$

where J = current density, A cm^{-2}

F = Faraday constant 96,500 coul $(g\text{-equiv})^{-1}$

Z = number of electrons involved in electrode reaction

D = diffusion coefficient of ionic species involved in electrode reaction, $cm^2\ sec^{-1}$.

t = time from start of constant-current passage, sec.

x = distance from electrode, cm.

$C_{(o,t)}$ = concentration, mol cm^{-3}, of ionic species at electrode ($x = 0$) at time t.

$C_{(x,t)}$ = concentration, mol cm^{-3} of ionic species at $x = x$, for time t.

C_b = concentration in bulk electrolyte, mol cm^{-3}.

Only the result for the electrode-electrolyte interface ($x = 0$) is usually needed, i.e.

$$\pm\left[C_{o,t} - C_b\right] = \frac{J}{zFD^{1/2}} \frac{2}{\pi^{1/2}} t^{1/2} \qquad (4.1\text{-}2)$$

where the plus sign is for the anode (from an expression comparable to Eq. 4.1-1 and the minus sign is for the cathode. It is convenient to consider the case of excess supporting electrolyte so that migration effects of the ionic species under consideration may be neglected for the present.

Combined Diffusion and Convection

Near to a vertical electrode, changes in the density of the electrolyte associated with the concentration changes give rise to buoyancy forces which tend to accelerate the electrolyte vertically upward for the cathode and downward for the anode. However, for vertical electrodes, Eq. 4.1-1 and 4.1-2 describe a fictitious behavior, since they imply that convection never commences. The acceleration imparted by the density changes is resisted by

inertial forces, chiefly designated in terms of the electrolyte viscosity, so that a frequent assumption is that Eq. 4.1-1 and 4.1-2 are valid for vertical electrodes for some time after the start of current passage. A generalized viewpoint regarding convection may be made as follows. The self-stirring due to natural convection supplies fresh material from the bulk of the solution to the vicinity of the electrode. The self-stirring, however, results from the density changes produced in an attempt to deplete (for the cathode) the electrolyte near the electrode. Hence, convection acts to slow down the progress of the depletion. For the anode, self-stirring aids in removing excess material from the region near the electrode, also slowing the attainment of a steady state distribution of concentration. Thus Eq. 4.1-1 and 4.1-2 may be regarded as a maximum limit for the case of natural convection combined with diffusion and must represent a fastest possible attainment of steady state conditions for the concentration and also the associated overvoltage at the electrode.

As a general result of fluid flow behavior for streaming past a surface, the velocity just at the surface drops to zero. Very close to the electrode, diffusional effects are thus expected to predominate so that even when the electrolyte undergoes density induced acceleration, the effect of convective supply will be least just at the electrode. Thus it may reasonably be expected that

Eq. 4.1-1 and 4.1-2 will agree closely with real behavior and will exactly describe conditions for sometime after the start of constant-current passage.

At steady state, for diffusion only, the ultimately attained concentration difference at x = 0 may be written as $\pm \left[C_{o,\infty} - C_b \right]$. From Fick's first law there is obtained, for the concentration variation within an imaginary finite boundary layer of thickness δ,

$$\frac{\left[C_{x,\infty} - C_b \right]}{\left[C_{o,\infty} - C_b \right]} = 1 - \frac{x}{\delta} \qquad (4.1\text{-}3)$$

Eq. 4.1-3, of course, cannot be valid in real cases since convection has been completely omitted. Interferometric[5] studies of steady state concentration contours (for $CuSO_4$ electrolytes) have shown that a semi-parabolic contour is actually followed to within a very good approximation. In terms of the δ implied in Eq. 4.1-3, with the same gradient at x = 0, the actual contour is given as

$$\frac{\left[C_{x,\infty} - C_b \right]}{\left[C_{o,\infty} - C_b \right]} = \left(1 - \frac{x}{2\delta} \right)^2 \qquad (4.1\text{-}4)$$

The contour of Eq. 4.1-4 also represents a particular von Karman-Pohlhausen approximation which has been used successfully as a "guessed" solution in many boundary layer problems for natural convection.

Similarity Domain

Equations 4.1-1 and 4.1-2 may be made dimensionless by introduction of the steady state result based on δ .

$$\pm\left[C_{0,\infty} - C_b\right] = \frac{J\delta}{zFD} \qquad (4.1\text{-}5)$$

and the dimensionless notation

$$\xi = \frac{x}{\delta} \; ; \quad \tau = \frac{Dt}{\delta^2}$$

Equation 4.1-2 for the absence of convection becomes

$$\frac{\left[C_{0,\tau} - C_b\right]}{\left[C_{0,\infty} - C_b\right]} = \frac{2}{\pi^{1/2}}\,\tau^{1/2} \qquad (4.1\text{-}6)$$

Thus normalization to the fraction of ultimate concentration difference at

$$x = 0 \quad (\xi = 0)$$

is possible for Sand's equation (Eq. 4.1-1, 4.1-2) by the introduction of the boundary layer thickness δ which is in turn based on an extrapolation of the actual gradient at x = 0.

A special case based on the boundary conditions

$$D\left|\frac{\partial C}{\partial x}\right| = \frac{J}{zF} \; ; \; x = 0 \; ; \; t \geq 0 \qquad (4.1\text{-}7a)$$

$$C = C_b \; ; \; x = \delta \; ; \; t \geq 0 \qquad (4.1\text{-}7b)$$

was worked out by Rosebrugh and Miller[6] in 1910.

The result involves a summation of exponential terms and may be improved for applicability at small times by solution of Equations 4.1-7a, 4.1-7b and the diffusion equation by the Laplace transform method. The result, after expansion of error function and exponential series terms is

$$\frac{[C_{o,\tau} - C_b]}{[C_{o,\infty} - C_b]} = \frac{2\tau^{1/2}}{\pi^{1/2}}\left[1 - e^{-\frac{1}{\tau}} + e^{-\frac{1}{\tau}}\left(1 - \frac{\tau}{2} + \frac{3\tau^2}{4} + \ldots\right)\right] \quad (4.1\text{-}8)$$

In terms of natural convection at a vertical electrode, the time variation of the contour resulting from the conditions given by Eq. 4.1-7a and 4.1-7b implies that when the diffusion "wave" reaches $x = \delta$, convection sets in suddenly and is maintained thereafter with full intensity. The fixed δ case of Eq. 4.1-8 may be regarded as equivalent to the no-convection situation described by Sand's equation (4.1-6) up to the time at which diffusion effects are felt at $x = \delta (\xi = 1)$. The attainment of ultimate concentration difference at $x = 0$ should be no more rapid than that described by Eq. 4.1-8 for the reasons given above in connection with Eq. 4.1-6. After $x = \delta$ has been reached, however, Eq. 4.1-8 describes a rather special behavior for natural convection in that a full stirring condition has been reached before it should be entirely possible. Thus, for a brief time after the "wave" reaches $x = \delta$, Eq. 4.1-8 should represent a <u>slow</u> extreme, with actual

systems attaining greater concentration differences in equivalent time. This behavior cannot be followed for a great length of time since Eq. 4.1-3 does not correspond to reality as time increases.

A plot of the limiting contours, Eq. 4.1-3, 4.1-4, together with Eq. 4.1-1 (dimensionless, cf. Eq. 4.1-5) for various τ in Figure 4.1-1 provides further physical insight to the problem. From Eq. 4.1-1 it may be readily computed that for a one per cent variation at $\xi = 1$ (i.e. a concentration fraction equal to 0.01), a dimensionless time of $\tau = 0.125$ is required. Thus the physical behavior underlying Eq. 4.1-6 and 4.1-8 is identical for $0 < \tau < 0.125$. A further period of identity between Eq. 4.1-6 and 4.1-8 may be found from the inner bracket of Eq. 4.1-8 expressed as the inequality

$$\frac{3}{4}\tau^2 - \frac{\tau}{2} \geq 0 \qquad (4.1\text{-}9)$$

The result obtained from Eq. 4.1-9 is that Eq. 4.1-6 and 4.1-8 are identical somewhere within the range $0 < \tau < 0.666$. From numerical computation of the appropriate functions, the range is narrowed to $0 < \tau < 0.333$ for one per cent agreement.

For real cases of concentration variation in electrolytes with low values of densification coefficient, $\alpha = \frac{1}{\rho}\frac{\partial \rho}{\partial C}$, and high values of kinematic viscosity, ν, it should be expected that the

onset of convection (acting to slow the attainment of ultimate concentration at $\xi = 0$) should be delayed. It is thus possible that real behavior could be described by Eq. 4.1-6 up to $\tau = 0.125$ and also for times beyond with Eq. 4.1-6 being a fastest possible mode of behavior. The fixed δ case would then represent a slowest possible mode up to some unspecified $\tau > 0.125$. Yet the results for both extreme modes (Eq. 4.1-6) fast and (Eq. 4.1-8) slow are identical up to $\tau \leq 0.333$. It seems plausible therefore that real behavior, lying between the extremes, must also be described over the range $0 < \tau < 0.333$. Beyond $\tau = 0.333$, the bracketing of real behavior can no longer be assumed either on the basis of the above calculations or physically. By substitution in Eq. 4.1-6 it may be seen that the concentration fraction attains a value of 0.4 at $\tau = 0.125$ and a value of 0.65 at $\tau = 0.333$. Thus, a substantial attainment of the ultimate concentration differenee is achieved in the time period for identity of the extremes. It should be emphasized that a real system might behave more slowly than Eq. 4.1-6 at all τ and that the circumstanee of faster attainment implied by Eq. 4.1-8 for some part of the interval $0.125 < \tau < 0.333$ might represent merely a fortuitous hypothetical situation. An estimate of such a possibility is shown as curve 6 of Fig. 4.1-2.

Curve A in Fig. 4.1-1 represents the linear contour extending over

the distance δ, ($0 < \xi < 1$) given by Eq. 4.1-3 as a result of the constraint imposed at δ by Eq. 4.1-7. Curve B represents a close approximation to the concentration contour observed in real systems for a comparable fixed gradient at $\xi = 0$ (cf. Eqn. 4.1-4). The contours at various values of τ represent the complete absence of convection. The shapes of the contours derived from Eq. 4.1-1 bear a superficial resemblance to the steady state contour of Curve B. In the absence of the complete solution, nothing can be said about the actual build up of the boundary layer to its ultimate thickness (2δ in Fig. 4.1-1), but a possible estimate might be made that the boundary layer does not extend very far beyond its steady state value during its transient behavior. The curve for $\tau = 0.5$ in Fig. 4.1-1 represents a condition of no convection up to a spreading of diffusion out to $\xi = 2$, ($x = 2\delta$) to within 1.5% on the concentration scale. The concentration fraction at $\xi = 0$ would have reached 0.8 in this time so that the stirring forces due to density changes would still not be fully developed. The sudden onset of convection at this space-time condition could be considered to stabilize the thickness of the boundary layer at $x = 2\delta$ with further density change within this region producing more stirring to slow down the attainment at $\xi = 0$. Such a possibility is shown at curve 3 in Fig. 4.1-2 purely on an estimated basis regarding the shape of the curve. The slowing down is the only certain feature, in that curve 3 of

Fig. 4.1-2 must be to the right of curve 1 (no convection). If convection were delayed until a concentration fraction of unity was achieved at $\tau = \pi/4$, information obtained at $\xi = 0$ from the concentration overvoltage could provide no indication of the readjustment of the contour to the steady state shape of curve B in Fig. 4.1-1. Curve 4 of Fig. 4.1-2 indicates this behavior. There is, of course, no reason why, with sufficiently weak density forces and large electrolyte viscosity, the concentration fraction of unity may be exceeded (except for the special case of cathode limiting current density) and thus also a spreading beyond the steady state boundary layer thickness. The period of adjustment of both concentration and distance to curve B of Fig. 4.1-1 is shown as the estimated curve 5 in Fig. 4.1-2.

A further estimate is possible for the case in which the diffusion wave is stopped at $\xi = 2$ by the commencement of convection. If diffusion alone were responsible for the readjustment from the curve for $\tau = 0.5$ to curve B in Fig. 4.101, the dimensionless time on the scale of Fig. 4.1-1 for the approach to steady state would be $\tau = 8$. This results from a general rule in all diffusion systems of finite extent and is related to the Einstein-Smoluchowski expression for Brownian movement,

$$x^2 = 2Dt \qquad (4.1\text{-}10)$$

In essence, the time required for a diffusing species to traverse the distance from $x = 2\delta$ to $x = 0$ as an average path should be associated with the termination of the diffusion process as a whole. This may be seen in Fig. 4.1-1 for the fixed δ, linear gradient case. However, for the $\tau = 0.5$ curve of Fig. 4.1-1, the slowing of concentration attainment beyond 0.8 would be accomplished by a nearly fully developed density change induced convection. No estimate is possible as to whether the combined convection and diffusion effects could proceed much further than $\tau = 8$, but this value should serve as a minimum time limit for steady state. The approach to steady state in all cases is asymptotic so that there is difficulty in exactly locating the terminal behavior. The estimated curve 3 in Fig. 4.1-2 is drawn with $\tau = 8$ as a limit. Note that the above reasoning implies a role for convection in which it is delayed up to $\tau = 0.5$ and is then practically fully established, leaving the task of contour readjustment to diffusion. Comparison of the behavior of actual systems with the estimated curves shown in Fig. 4.1-2 should afford some insight into the effect of convection in the overall exact transient problem. A brief summary of Eq. 4.1-6 and 4.1-8 is given for various selected value of τ in Table 4.1-1

TABLE 4.1-1

$$\frac{C_{(0,t)} - C_b}{C_{(0,\infty)} - C_b}$$

τ	Pre-existing δ Eqn. 4.1-8	Pure Diffusion Eqn. 4.1-6
.001		0.0357
.005		0.0798
.01		0.1128
.05		0.2548
.1		0.3568
.15		0.4370
.2	0.5041	0.5046
.3	0.6132	0.6180
.4	0.6979	0.7136
.5	0.7639	0.7979
.6	0.8156	0.8740
.7	0.8559	0.9440
.8	0.8874	1.0092
.9	0.9120	1.0705
1.0	0.9312	1.1284
1.5	0.9800	1.3820
2.0	0.9942	1.5958
3.0	0.9995	1.9544

Limitations

It is implicit in the present analysis that the diffusion coefficient is independent of concentration and, for the thermal analog, that the fluid thermal diffusivity is independent of temperature.

Also, since Eq. 4.1-6 and 4.1-8 are based on linear diffusion, due caution should be exercised in applying the present analysis to natural convection systems near the leading edge of the electrode (upper edge for vertical anode, lower edge for cathode) where the greatest variation of the actual δ with distance along the electrode is to be found.

References

1. R. J. Goldstein, E.R.G. Eckert, Int'l J. Heat Mass Transfer V. 1, p. 208-218, 1960.
2. B. Gebhart, Paper 60-HT-33, ASME - AIChE Heat Transfer Conference, Buffalo, N. Y., Aug. 15-17, 1960.
3. H. F. Weber, Wied. Annalen, V7, p. 536, 1879.
4. H. J. S. Sand, Phil. Mag. V1, p. 45, 1901.
5. N. Ibl, Eighth Meeting CITCE 1956, Butterworths, London, p. 172.
6. T. R. Rosebrugh, W. L. Miller, J. Phys. Chem., V. 14, p. 816, 1910.

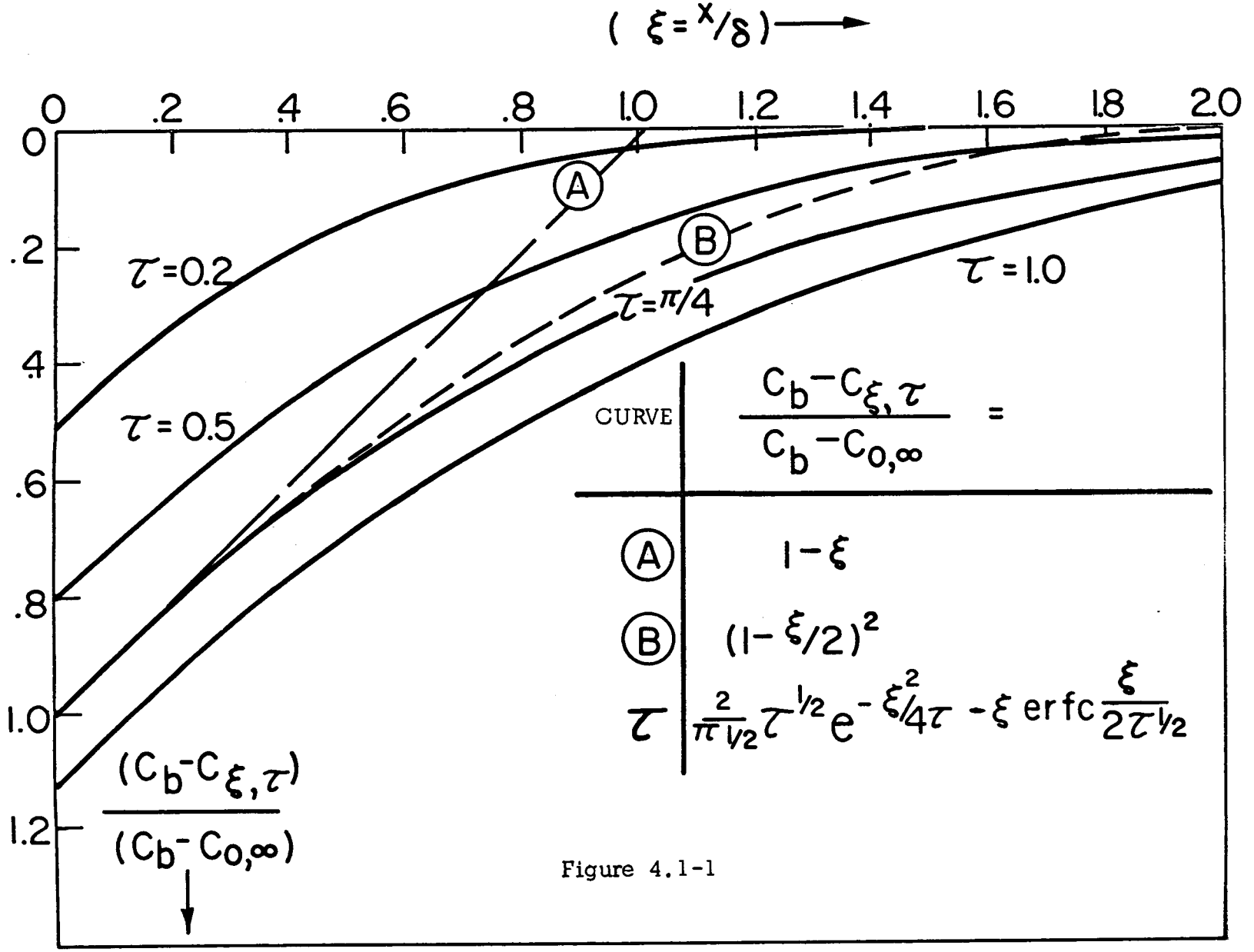
(ξ = x/δ) ⟶
0
.2
.4
.6
.8
1.0
1.2
1.4
1.6
1.8
2.0
A
B
τ = 0.2
τ = 0.5
τ = π/4
τ = 1.0
CURVE
$\frac{C_b - C_{\xi,\tau}}{C_b - C_{0,\infty}}$ =
A
1 − ξ
B
$(1 - \xi/2)^2$
τ
$\frac{2}{\pi^{1/2}} \tau^{1/2} e^{-\xi^2/4\tau} - \xi \operatorname{erfc} \frac{\xi}{2\tau^{1/2}}$
$\frac{(C_b - C_{\xi,\tau})}{(C_b - C_{0,\infty})}$

Figure 4.1-1

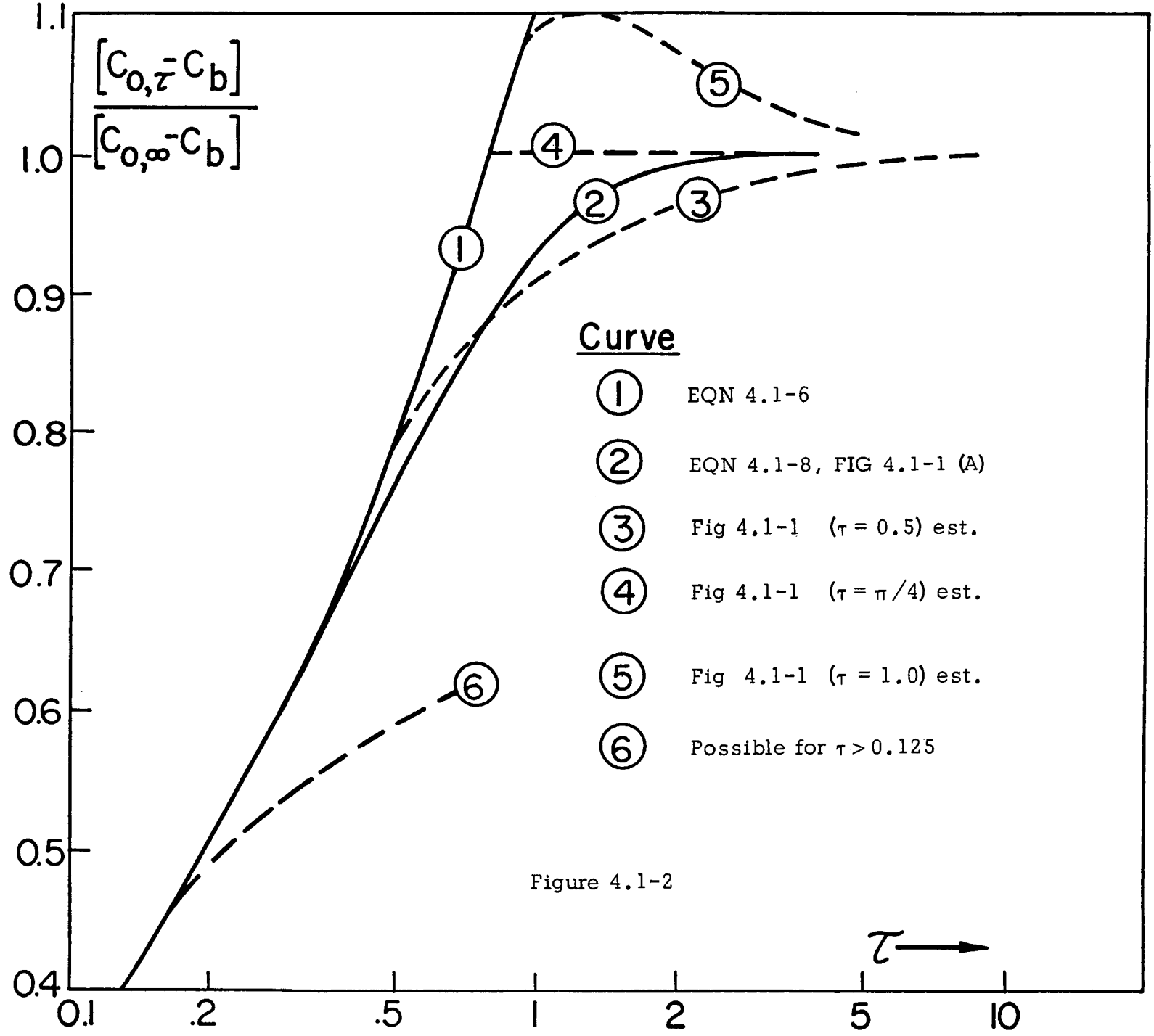
1.1
1.0
0.9
0.8
0.7
0.6
0.5
0.4
$\frac{[C_{0,\tau} - C_b]}{[C_{0,\infty} - C_b]}$
0.1
.2
.5
1
2
5
10
τ
Curve
1 EQN 4.1-6
2 EQN 4.1-8, FIG 4.1-1 (A)
3 Fig 4.1-1 ($\tau = 0.5$) est.
4 Fig 4.1-1 ($\tau = \pi/4$) est.
5 Fig 4.1-1 ($\tau = 1.0$) est.
6 Possible for $\tau > 0.125$

Figure 4.1-2

5. LIST OF PUBLICATIONS

INDEC-1 H. Yeh and T. K. Chu, "The Optimization of MHD Generators with Arbitrary Conductivity," ASME Paper 63-WA-349.

INDEC-2 M. Altman, D. P. Ross, H. Chang, "The Prediction of Transient Heat Transfer Performance of Thermal Energy Storage Devices," paper presented at the 6th National Heat Transfer Conference, Boston, Mass., Aug. 11-14, 1963.

INDEC-3 G. R. Belton and Y. K. Rao, "The Binary Eutectic as a Thermal Energy Storage System: Equilibrium Properties," paper presented at the 6th National Heat Transfer Conference, Boston, Mass., Aug. 11-14, 1963.

INDEC-4 J. Dunlop and G. Schrenk, "Theoretical Model of a Thermionic Converter," Proceedings of Thermionic Specialized Conference, Gatlinburg, Tenn., Oct. 7-9, 1963, pp. 57-62.

INDEC-5 R. Sharma and H. Chang, "Thermophysical and Transport Properties of High Temperature Energy Storage Materials," paper presented at the Third Annual Symposium, High Temperature Conversion Heat to Electricity, Tucson, Arizona, Feb. 19-21, 1964.

INDEC-6 G. L. Schrenk, "Solar Collection Limitations for Dynamic Converters-Simulation of Solar-Thermal Energy Conversion Systems," Proceedings of AGARD Conference, Cannes, France, March 16-20, 1964.

INDEC-7 M. Altman, "Prospects for Thermal Energy Storage," Proceedings of AGARD Conference, Cannes, France, March 16-20, 1964.

INDEC-8 M. Altman and G. Schrenk, "An Approximate Analysis of Ablation on a Composite Slab," AIAA paper.

INDEC-9 L. Zelby, "The Hollow Thermionic Converter," IEEE Annual Meeting on Energy Conversion, Clearwater, Florida, May, 1964.

INDEC-10 M. Altman, "The Institute for Direct Energy Conversion," paper presented at Am. Soc. Eng. Ed. Annual Meeting, University of Maine, Orono, Maine, June 22-26, 1964.

INDEC-11 G. Schrenk, "Emitter Sheath Polarity in Plasma Diodes, "The Proceedings of Thermionic Specialist Conference, Cleveland, Ohio, Oct. 26-28, 1964, pp. 249-257.

INDEC-12 M. Kaplit, G. Schrenk, L. Zelby, "Electron Emission from Metals in Gaseous Environment," Proceedings of Thermionic Specialist Conference, Cleveland, Ohio, Oct. 26-28, 1964, pp. 4-10.

INDEC-13 G. Schrenk, "Criteria for Emitter Sheath Polarity in Plasma Diodes," paper presented at ASME Winter Annual Meeting, New York, Nov. 29 - Dec. 3, 1964.